Rediation and Eddy Flux Experiment 1991 *(REFLEX I)*

Jörg Hartmann, Christoph Kottmeier und Christian Wamser

Ber. Polarforsch. 105 (1992)
ISSN 0176 - 5027

Jörg Hartmann, Christian Wamser, Christoph Kottmeier

Alfred-Wegener-Institut für Polar- und Meeresforschung
Columbusstraße
D-2850 Bremerhaven
Bundesrepublik Deutschland

Contents

Abstract iii

1 Introduction 1

2 Experimental Phase 3

3 The *Polar 2* Aircraft Instrumentation 5

3.1 The *Polar 2* aircraft 5

3.2 Basic Facility 5

3.3 The Meteopod Turbulence Measuring System 6

3.4 Line Scan Camera 7

3.5 Dropsonde 8

4 Sensor Calibration 9

4.1 Lyman-alpha Humidiometer 9

4.2 Wind Velocity 9

4.3 Temperature Sensors 11

4.4 Radiation Thermometer 11

5 Flight Catalogue 13

6 Data Presentation 48

6.1 Contrast in Turbulence over Sea Ice and Open Water 48

6.2 Roll Vortex Motion 51

6.3 Analysis of Surface Structure from LSC Data 57

6.4 Relation between Surface Structure and Airborne Measurements . . . 70

7 Acknowledgements 72

8 References 72

List of Figures

1 Calibration of Lyman alpha humidiometer. 10

Catalogue of flights. For each of the 17 flights a schematical sketch of the flight path together with an ice chart and a sketch of the flight pattern are given. 14

2 Time series of θ', q' and w' for two 12 km sections of a level flight in 30 m height on 28 Sep 91. 49

3 Spectra of w', θ' and q' for two 12 km sections of a level flight in 30 m height on 28 Sep 91. 50

4 Cospectra of $w'\theta'$ and $w'q'$ for two 12 km sections of a level flight in 30 m height on 28 Sep 91. 51

5 Spectra of turbulence quantities for three runs over open water (Figures a–c) across roll circulation on 14 Oct 91. 53

6 Time series of potential temperature, specific humidity and the wind components. 56

7 A series of Line Scan Camera pictures (a-h) showing different sizes, concentrations and structures of ice floes. 58

8 Percentage of open water, nilas and ice as a function of distance from ice edge. 67

9 Distribution of floe sizes, corresponding to Figures 7 c, d, e, f. 68

10 Characteristic floe sizes parallel and orthogonal to the flight direction as a function of distance from the ice edge. 69

11 Time series of radiation, turbulent fluxes and water coverage. 71

List of Tables

1 Atmospheric parameters for low level runs on 28 Sep 91. 48

2 Atmospheric parameters for the cross wind runs on 14 Oct 91. 52

Abstract

An aircraft based study of interactions between sea ice and the atmospheric boundary layer was conducted in early autumn 1991 in the marginal ice zone north of Svalbard (15°E 78°N). The aircraft was equipped with turbulence and radiation instruments and carried a high resolution Line Scan Camera (LSC) to record digital images in the visible range of the ice and new ice (nilas) concentration. Seventeen flights, under a range of different synoptic and ice conditions, were conducted with flight patterns arranged to study low-level turbulence over different ice conditions, radiative fluxes below and above clouds and convective structures downstream of the ice edge.

This report outlines the scientific objectives and describes the instrumentation and the experimental phase. It comprises a catalogue of all flights and presents examples of typical features measured during the campaign.

1 Introduction

The *Radiation and Eddy Flux Experiment,* REFLEX I, was conducted north of Svalbard (15°E 78°N) on the basis of aircraft measurements to study processes in the atmospheric boundary layer above Arctic sea ice. Within the context of possible changes of sea ice extent and thickness in the Arctic, the programme aims to better determine the relationships between the state of sea ice and evolution of the atmospheric boundary layer. Flight patterns were arranged to obtain data for experimental studies of boundary layer processes and for related numerical model studies.

The objective is to study the interaction between the sea ice covered ocean surface and the atmospheric boundary layer (ABL). The interaction is potentially strong, since radiative and turbulent exchange processes contribute to the melting and freezing of sea ice and to changes of ice concentration due to wind driven compaction and divergence of the ice. The state of the sea ice in turn determines the boundary condition for the lower atmosphere. Ice concentration and floe size distribution characterise the roughness and temperature inhomogenity of the surface. Turbulent exchange of heat, momentum and moisture plays a key role in the formation of low stratus clouds, which in turn, influence considerably radiative fluxes at the surface.

Since the vertical exchange of momentum and energy vary considerably with ice concentration and thickness, a major objective of the programme is to derive parameterisations for fluxes in relation to sea ice statistics. Turbulent fluctuations of wind, temperature and humidity, as well as their mean values, were measured during some 40 flight legs at altitudes of about 30 m. Turbulent fluxes of heat, humidity and momentum determined from the Meteopod data are then related to floe size and edge statistics from LSC data.

Fetch dependence of turbulent fluxes of heat, momentum and moisture are studied by flights downstream of pronounced surface temperature inhomogenities, the most significant of which is at the ice edge under off-ice wind conditions. In this region, shallow layer convection frequently organises into vortex rolls. Vertical profiles of wind, temperature and humidity were determined to derive the boundary conditions for roll formation.

Flight patterns, consisting of flight legs at different heights in the ABL, provided the vertical structure of the atmospheric mean and turbulent quantities. Short- and longwave radiation measurements from below and above clouds gave information on the shortwave cloud transmissivities and effective longwave emissivities. From aircraft ascents and descents cloud liquid water content was estimated. The flights cover a wide range of wind speeds, atmospheric stabilities, cloud and ice conditions.

The evolution of the ABL structure, stratus clouds and ice conditions were observed by several successive flights into the same area with similar flight patterns. In the absence of synoptic scale advection, individual contributions to the heat and moisture budget of the ABL including the formation of stratus clouds are derived.

Parameterisation of ABL quantities requires information on the large scale state of sea ice and atmosphere. For that purpose, two meteorological/oceanographic buoys were been deployed on ice floes prior to the experiment. The buoys supply data to monitor ice motion, ice thickness, oceanic mixed layer variations and atmospheric pressure. The latter is incorporated in the routine surface pressure analysis. Information on ice concentrations were obtained from high altitude LSC flights and High Resolution Picture Transmission (HRPT) imagery of the Advanced Very High Resolution Radiometer (AVHRR) satellite.

This report covers a brief description of the aircraft instruments and their calibration in sections 3 and 4, and a catalogue of flights with flight patterns, cloud and ice concentrations in section 5. Examples of turbulence data obtained by the turbulence probe system Meteopod, ice observations with a Line Scan Camera and radiation data are presented in section 6.

2 Experimental Phase

The experiment took place from September 16th to October 17th, 1991. During missions, the instruments were operated by scientists of the Alfred-Wegener-Institut für Polar- und Meeresforschung (AWI) and engineers of Aerodata GmbH, Braunschweig. The *Polar 2* was flown by pilots of the *Deutsche Forschungsanstalt für Luft- und Raumfahrt* (DLR) and Aerodata. Most of the aircraft scientific equipment has been installed by Aerodata, the Line Scan Camera was developed by AWI (Wamser and El Naggar, 1989; Bochert, 1991).

All flights were planned in a temporary office of the *Norsk Polar Institutt* at Longyearbyen Lufthavn. Weather information was available from the meteorologist of *Det Norske Meteorologiske Institutt* (DNMI) at Longyearbyen and from maps received by fax. Actual satellite information was restricted to screen displays of data from the polar orbiting NOAA satellites. Additional weather information from the sea ice zone was available from two buoys deployed by AWI to the northeast of Svalbard and from *Polarstern* and *Oden*, two ice-breaking research vessels that operated between Svalbard and the North Pole.

All aircraft operations took place in the area between 5°E 78°N and 25°E 83°N, most of them north of Svalbard. The catalogue of flights (Section 5) shows the individual flight paths. Under typical mission requirements which included operators, scientific equipment and mandatory polar survival gear the aircraft had an endurance of 6.5 hours. Two hours had to be retained as a reserve, since no alternate landing field was available in the region. The ferry flights to and from the area of the experiment took a further two hours, leaving roughly 2.5 hours for operations over the ice. With the nominal speed for turbulence measurements of 70 m/s this corresponds to an availability of some 600km for flight patterns.

Flight patterns belonged to one of the following basic types:

I LSC survey flights at altitudes of 1000 m and greater for studies of ice type distribution, concentration and floe size distribution

T Low level flights at an altitude of 30 m for studies of turbulent fluxes of momentum, heat and moisture above different ice categories. LSC data are also available for most of these low level flights.

BLP Boundary layer flight patterns with 30 km long legs at different heights between 30 m and above the tops of stratus clouds, conducted for studies of the vertical structure and evolution of the ABL and radiation fluxes over sea ice.

W Ice edge flight patterns at different heights crossing the sea ice/open water boundary during off-ice winds, to study the fetch dependence of turbulent fluxes over open water.

Patterns I and T were flown over distances of 50 to 200 km across the marginal ice zone up to the most northerly position of 83°N, were multiyear floes were regularly found. The observations thus covered a wide range of different ice conditions. If not impeded by clouds, a high level flight was combined with a low level flight back.

Turbulence data are available for a total of 3500 km of level flights, 1800 km of which were flown at an altitude of 30 m (pattern T). LSC data over a total of 4600 km at different heights cover an area of 3000 km^2. The BLP-pattern was flown in 12 situations over sea ice and the W-pattern was flown four times over the open water during cold air outbreaks.

3 The *Polar 2* Aircraft Instrumentation

During REFLEX I four different instrumentation systems were flown on the *Polar 2* aircraft, each having its own data aquisition and recording facility.

These systems were:

The *Basic Facility*, recording data at 10 Hz from slow response sensors and from the aircraft's positioning system. All data can be calibrated on-line and displayed as physical values, alphanumerically or graphically.

The *Meteopod* turbulence system, recording data at 50 Hz from flow sensors, fast response temperature and humidity sensors, and the aircraft's positioning and attitude information. As for the Basic Facility data can be monitored on-line.

The *Line Scan Camera* which provided a high-resolution digital image of the flight path in the visible range to obtain ice information.

The *Dropsonde* system, employing Vaisala radio sondes which provided wind information based on the Omega navigation system, along with temperature, humidity and pressure.

3.1 The *Polar 2* aircraft

The *Polar 2* research aircraft is a Dornier DO228 turbo-prop 9-seater with a wing span of 17 m and a length of 15 m. It is fully IFR-equipped and has a laser-gyro Inertial Navigation System (INS). For REFLEX I a Global Positioning System (GPS) was also available. Although it is equipped with a de-icing system, *Polar 2* cannot be operated under icing condition if the Meteopod turbulence system is mounted. Generally, missions were flown with a five person crew, two pilots, one or two operators and one or two scientists.

3.2 Basic Facility

3.2.1 Positioning Information

All relevant positioning information from the aircraft's laser gyro INS was recorded at 10 Hz. GPS positioning data was provided by an SEL 6 channel receiver, at a rate of roughly 1 Hz. The INS data were used for the on-line wind calculation of both the Basic Facility and the Meteopod, GPS data were decoded and displayed in the basic equipment, but not incorporated in the on-line wind calculation.

3.2.2 Surface Temperature

Surface temperature was measured by a Heimann KT4 radiation thermometer with a sensitivity in the range of 8 to 14 μm. This range coincides with the atmospheric window where the influence of absorption by water vapour for long measuring distances is reduced. The opening angle of 0.6° corresponds to a ratio of distance to field diameter of 100:1. The response time is 0.1 s (to 90% of the final value). The KT4 could be calibrated in-flight by moving a black-body radiator in its path.

3.2.3 Radiometers

Upward and downward looking Eppley pyranometers and pyrgeometers were mounted above the fuselage between the wings and under the fuselage in the tail section, respectively. The mounting positions were optimised to keep possible effects due to shading by parts of the aircraft like rudder or landing gear to a minimum. The mounting plates were thermally insulated to prevent influences on the thermopiles by the aircraft's air conditioner. The pyrgeometers consist of thermopiles shielded by a silicone hemisphere with a transmittance in the 4 to 40 μm spectral range. The radiometers were calibrated prior to the experiment at the Instrumentenamt des Deutschen Wetterdienstes in Hamburg.

3.2.4 Temperature and Humidity

In addition to the turbulence sensors in the Meteopod a de-iceable Rosemount total-temperature sensor (Pt100) and a Vaisala-Humicap mounted inside a Rosemount housing (Aerodata) were carried at the fuselage and recorded at 10 Hz. The temperature sensor has a range of ±50°C, an absolute accuracy of 0.3°C and a resolution of 0.05°C. Similarly the humidity sensor values are 0.0–100%, ±0.05% and 0.05%, respectively. More detailed description of the instruments can be found by Vörsmann, *et al.,* 1989.

3.3 The Meteopod Turbulence Measuring System

The turbulence sensors were mounted in a pod under the right wing of *Polar 2*. The system is described in detail by Vörsmann, *et al.,* 1989, only a brief overview of the most important instruments is given here.

3.3.1 Positioning Information

Aerodynamic forces on the wing may generate high-frequency motion of the flow probes that are different to those that the fuselage-bound INS records. In order

to accurately sense this motion a separate *Attitude and Heading Reference System* (AHRS), a Litton LTR 81, is placed in the Meteopod, as close as possible to the flow probes. From this AHRS the vertical acceleration and the angles of roll (ϕ) and pitch (θ) were used for the on-line calculation of the wind vector. The low period vertical movement was derived from the measurement of the static pressure. The horizontal velocity components are taken from the laser-gyro INS.

3.3.2 Humidity Measurements

The Meteopod carried the aircraft-version of the A.I.R. Lyman-alpha humidiometer and a dew-point mirror to provide an absolute reference. A third humidity instrument was a Vaisala-humicap inside a Rosemount-housing (Aerodata). This is the same instrument as the one mounted on the fuselage.

3.3.3 Flow Sensors

At the tip of the Meteopod, roughly 1.5 m in front of the leading edge of the wing, a de-iceable 5-hole-probe provided angle-of-attack, angle-of-sideslip, airspeed and static pressure. The pressures were measured with Rosemount transducers, placed in a very short distance to the probe to avoid attenuation by long tubes.

3.3.4 Temperature Sensors

Three temperature sensors were mounted on the Meteopod, all with a Pt100 sensing element.

- An original Rosemount E-housing.
- A modified Rosemount housing (Aerodata) that carried also the Vaisala-humicap.
- A newly designed, very fast reverse-flow housing which had a sensing element that consists of 44 cm of 0.025 mm diameter Pt-wire wound around three very light rods of delrin material. The rods form an open triangle with a 1 cm side length. The sensing element sits inside a cylindrical body open at its rear end and made of styrofoam to avoid any thermal influences of the housing on the sensor.

3.4 Line Scan Camera

High resolution digital data of the ice/nilas concentration were sampled by a vertically downward looking *Line Scan Camera* (LSC) system on several tracks of the 17 flights. The system was developed at the AWI for quantitative measurements

of the ice concentration and floe size distribution (Wamser and El Naggar, 1989, Bochert, 1991). The Camera has an opening angle of 56° and records one line of 1024 pixels every 30 milliseconds. Each pixel has an eight-bit value that corresponds to the intensity in the visible range (400 to 900 nm) of the reflected sunlight. The spatial resolution of the system depends on the flight velocity (x-direction) and on the height of the aircraft for the cross direction (y). For a height of 1000 m and a speed of 70 m/s an ice floe of about 2 m^2 can be resolved.

3.5 Dropsonde

A Vaisala Marwin MW12c radio sonde system was installed on two days of the experiment. Sondes of the type RS 80-15 N were released on parachutes with a sink rate of 7 m/s from heights of 3000 m and 3600 m above ground. Omega/VLF signals received by the sondes are relayed on a 400 MHz carrier to the Marwin, where they are processed to derive the sondes' movements based on relative phase shifts. Pressure, temperature and humidity are sampled every 2 seconds, wind data are available in 10 seconds intervals. Omega wind information is available for only one day.

4 Sensor Calibration

The instrumentation and data processing facilities in *Polar 2* were designed and set up to provide real-time physical values of all measured quantities in a final form, including calibration and correction procedures. This worked satisfactory for nearly all instruments or derived quantities. In a few cases, however, sensors were found to need a recalibration, or derived quantities needed a recalculation. This applies to the lyman-alpha humidiometer, the temperature sensors, the vertical wind velocity and the KT4 infrared radiometer. This section describes the applied procedures.

4.1 Lyman-alpha Humidiometer

The A.I.R.-Lyman-alpha is a fast-response, accurate and absolute instrument that is stable over a period of several tens of hours, but drifts slightly during the lifetime of the emitter and receiver tubes. More important, the path length needs to be adjusted for the given humidity conditions to achieve an optimum resolution. Therefore, a recalibration is usually necessary for each experiment. For REFLEX I the range was set to cover $0 \leq \rho_v \leq 8\,\mathrm{g/m^3}$.

In the implemented on-line calibration procedure the Lyman-alpha was bound to the Vaisala humicap. The measurement of absolute humidity by the dewpoint mirror, however, are in most cases of higher accuracy. Therefore the output voltage of the Lyman-alpha was recalibrated. For all flights the relation $\rho_v = 2.30345 - 0.43678\,U$, where ρ_v is the water vapour density in $\mathrm{kg/m^3}$ and U the output voltage of the lyman-alpha, is used. This calibration was derived from several ascent and descent flights, where a large range of humidity variations occurred. Figure 1 shows an example. Note that several step-like deviations from the calibration curve are generated by the fast response of the lyman-alpha to a rapid change, and the slow adaption of the dew-point mirror.

4.2 Wind Velocity

The measurement of the three-component wind vector from an aircraft requires the accurate determination of the vector of the aircraft motion relative to the air $\vec{A}$ and relative to the earth $\vec{G}$. The wind vector results as the difference $\vec{V} = \vec{G} - \vec{A}$. Under nomal conditions the wind vector is small with respect to $\vec{G}$ and $\vec{A}$, therefore small errors in $\vec{G}$ and $\vec{A}$ result in large errors in $\vec{V}$.

In *Polar 2* the horizontal components of $\vec{G}$ are determined by the INS mounted in the fuselage and the vertical component by adding the high-pass filtered integrated acceleration measurement of the AHRS to the low-pass filtered differentiated static pressure.

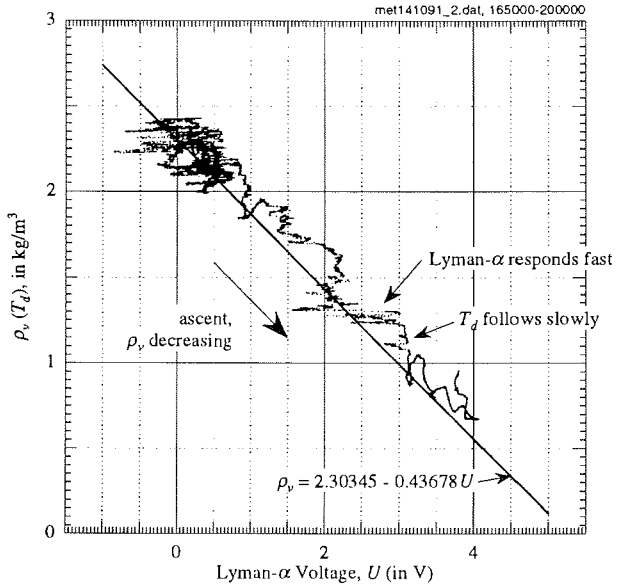

Figure 1: Calibration of Lyman alpha humidiometer. Data are from an ascent from 30 m to 3000 m on 14 Oct 91. The solid line is $\rho_v = 2.30345 - 0.43678\,U$.

The AHRS, however, is subject to offsets in attitude angles of up to one degree, generated by each turn flown between horizontal flight legs. These offsets disappear gradually over a period of approximately five minutes. Furthermore, in the on-line wind calculation, the gain functions of the applied filters did not perfectly add to one over the entire frequency range.

Therefore, the vertical wind component has been recalculated from the measurements of the 5-hole probe and the AHRS. Acausal filters with high- and low-pass gain functions $G_h(f)$ and $G_l(f)$ such that $G_h(f) + G_l(f) = 1$, for all f, were applied in the Fourier domain to the integrated acceleration and differentiated pressure, respectively.

The angle offset results in an offset of the obtained vertical velocity component which has been removed by subtracting a linear regression from the data series. More elaborate correction schemes for this AHRS error are possible, but do not result in better measurements of w, especially for length scales of less than five kilometres.[1]

[1] Unfortunately the acceleration and attitude data of the INS were not recorded in the meteopod data stream. They are recorded in the data stream of the basic facility, but the synchronisation of these two streams is not sufficiantly accurate.

4.3 Temperature Sensors

The Platinum wire temperature sensors in the Rosemount housings are standard Pt100 sensors with an accuracy of ±0.25°C. They were calibrated in a fluid bath by the *Physikalisch-Technische Bundesanstalt* in Braunschweig, Germany. The recording electronic was carefully calibrated with a precision Pt100 simulator. The influence of adiabatic heating on the temperature measurement is removed with coefficients that have been found in extensive wind tunnel test by Rosemount Inc.

However, comparison flights with the DLR-Falcon in September 1990 indicate that the meteopod temperature measurements are approximately 1 K lower than those of the Falcon.[2] Comparison with an Assmann psychrometer on 28 September 1991 at the airfield in Longyearbyen also showed lower temperatures for the airborne equipment (-0.95 K for the meteopod E-housing and -0.917 K for the E-housing of the basic equipment, both are averages over several measurements). The reason for this disagreement needs still to be found. As both comparisons, in-flight and ground-based, show similar offsets the problem does not seem to be with the airspeed correction.

The offset is corrected by adding the differences found by the comparison with the psychrometer.

The sensing element of the fast reverse flow sensor is not a standard Pt100, but has a resistance of $R_0 = 93.4818\,\Omega$ at 0°C. The temperature is then computed according to DIN-IEC 751:

$$T = \frac{A}{2B} - \sqrt{\left(\frac{A}{2B}\right)^2 - \frac{1 - \frac{R}{R_0}}{B}}$$

where $A = 3.90802{\cdot}10^{-3}K^{-1}$, $B = -0.580195{\cdot}10^{-6}K^{-2}$ and $R = R(T)$ the resistance at temperature T.

4.4 Radiation Thermometer

During flights the KT4-radiation measurements were calibrated on 26 occasions with a black body radiator moved into the optical path. The black body temperatures were evenly distributed between −6 and +10°C. Since the temperatures of the radiation thermometer showed a systematic deviation from those of the black body, a correction

$$T_{KT4,c} = 0.9\,T_{KT4,m} + 1.14\,\mathrm{K}$$

was applied, where $T_{KT4,m}$ denotes the observed and $T_{KT4,c}$ the corrected surface temperature, both in °C.

[2] During the comparison with the Falcon the Meteopod was carried by the Polar 4 which has its own basic equipment. The temperature measurements of that basic equipment, however, were also approximately 1 K lower.

The corrected surface temperatures were shown to be compatible with observations of the ocean surface at freezing temperatures, which were identified by careful inspection of the ice observations. The error can be due to an insufficient temperature correction of the KT4-measurements since the internal compensation applies only to temperatures above +10°C.

5 Flight Catalogue

The following catalogue presents schematical sketches of flight paths, flight patterns, and brief summaries on cloud and ice conditions from all missions.

Flight patterns indicate the altitudes and the horizontal extent of the flight legs in a vertical plane. Observed cloud top and bottom heights and information on the ice concentration from LSC observations are shown schematically. Availability of data from the Line Scan Camera and the Meteopod is indicated by LSC and MP, respectively. The *Basic Facility* was recorded continuously on all flights. The abbreviation TEMP represents measurements to determine vertical profiles of wind, temperature and humidity, and BLP boundary layer patterns, respectively. Sea ice is plotted as a thick line at the surface.

Flight paths are shown together with ice concentration maps derived from weekly NOAA ice charts. Ice maps are updated about once a week, thus the dates of the flights may deviate up to 4 days from that of the ice analyses. Additionally ice edges were located according to aircraft positions. Arrows in the upper right give the initial and final positions of two buoys (No. 9361 and 9355) during the period indicated at the bottom of the figure. Ice concentrations are indicated by isolines marking the areas of >9, 7-9, 4-7 and 1-4 tenth of coverage.

For each flight the start and end of the Meteopod recording is given in local time.

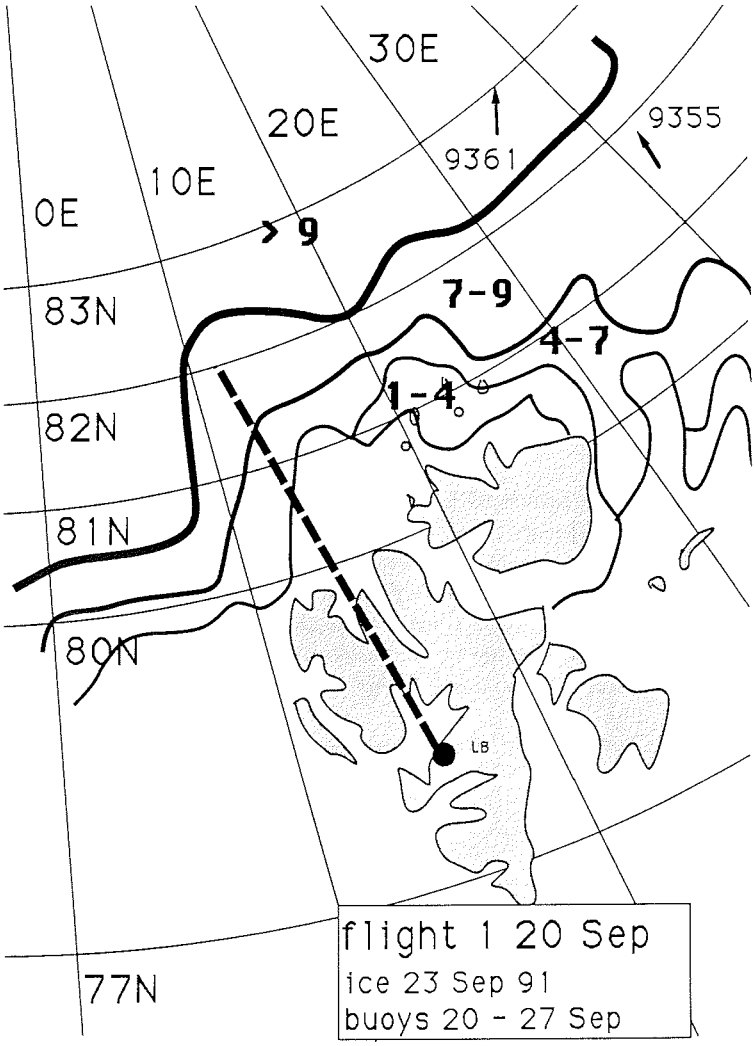

Flight 1, 20 Sep 91, 14:22–16:03

In front of a low pressure system, situated to the southwest of Svalbard, warm air with temperatures slightly above 0°C in the boundary layer was transported over the marginal ice zone by moderate southerly winds. Cloudless conditions prevailed over the sea ice, northward of 82°N a shallow stratus cloud cover was present.

The almost cloudless condition were used for a northbound flight at an altitude of 1000 m for an ice survey with the LSC. The return flight at low altitudes provided a check on the turbulence instrumentation and turbulent fluxes under a weak thermal stability.

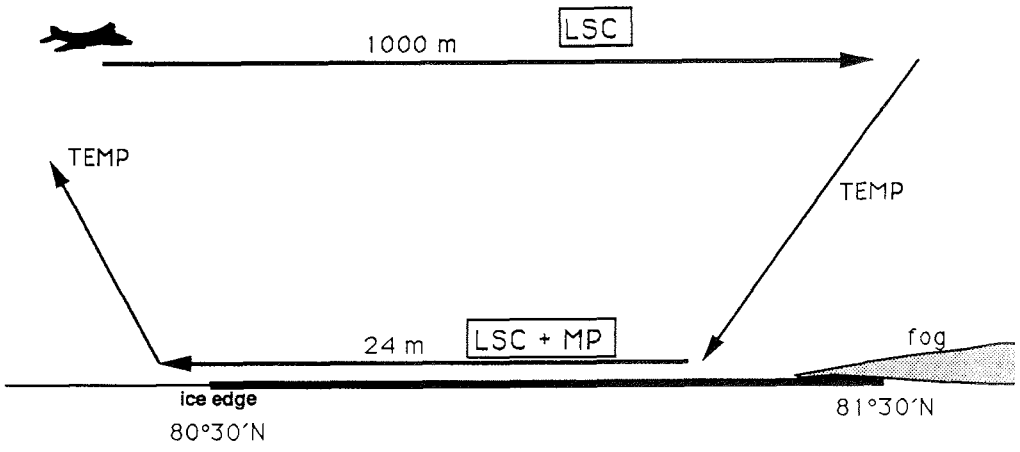

FLIGHT : 20 Sept 91

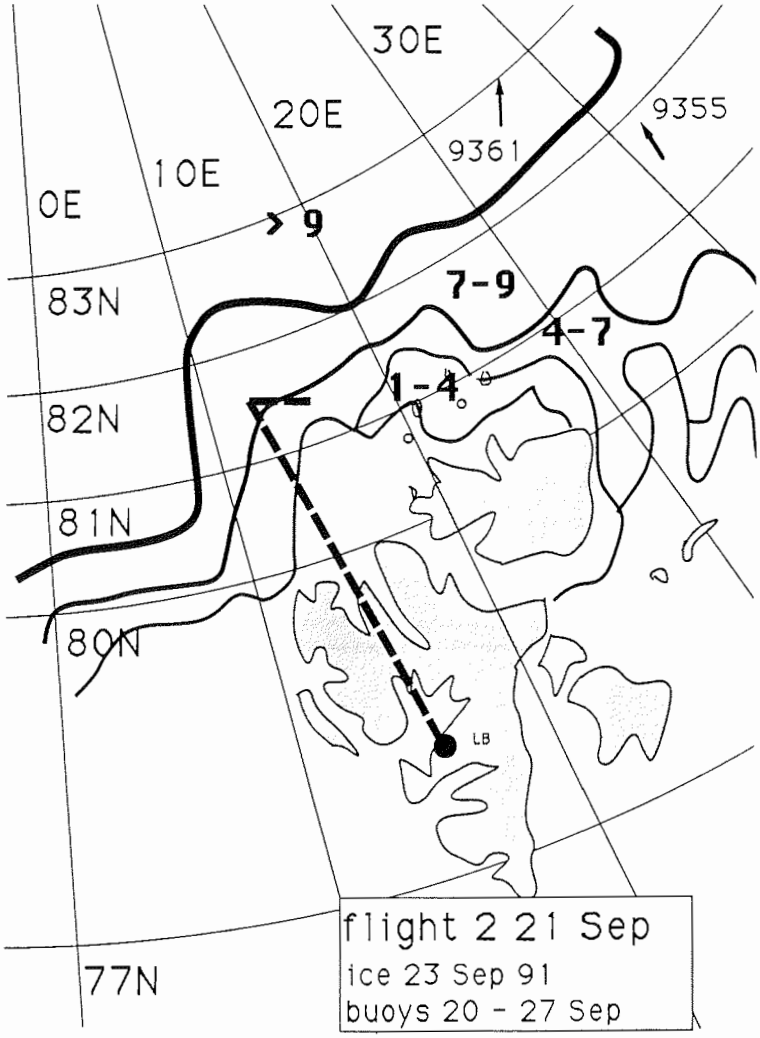

Flight 2, 21 Sep 91, 10:35–13:21

A moderate southerly flow advected maritime air over the sea ice. The cloud distribution was as follows: 8/8 altocumulus between 1700 m and 2300 m, and 5/8 to 8/8 stratocumulus between 800 m and 1800 m.

The flight consisted of an ice survey flight beneath the lowest clouds (580 m) to a point 81°30′N and a low-level flight back on the same route (30 m height) with turbulence measurements. A boundary layer pattern in between was flown to detect the vertical structure of the turbulent and radiation fluxes in the presence of Arctic stratus clouds.

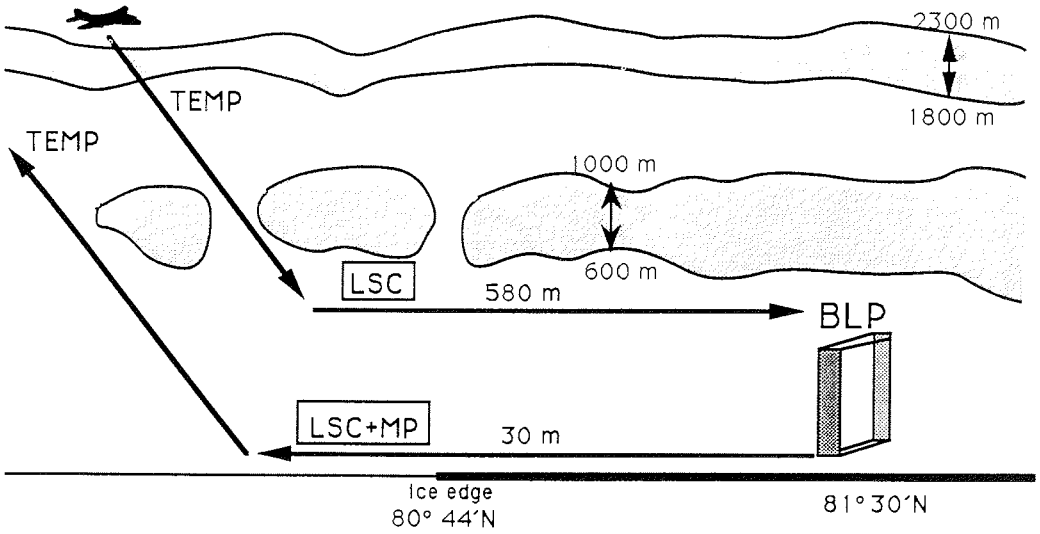

FLIGHT: 21 Sept 91

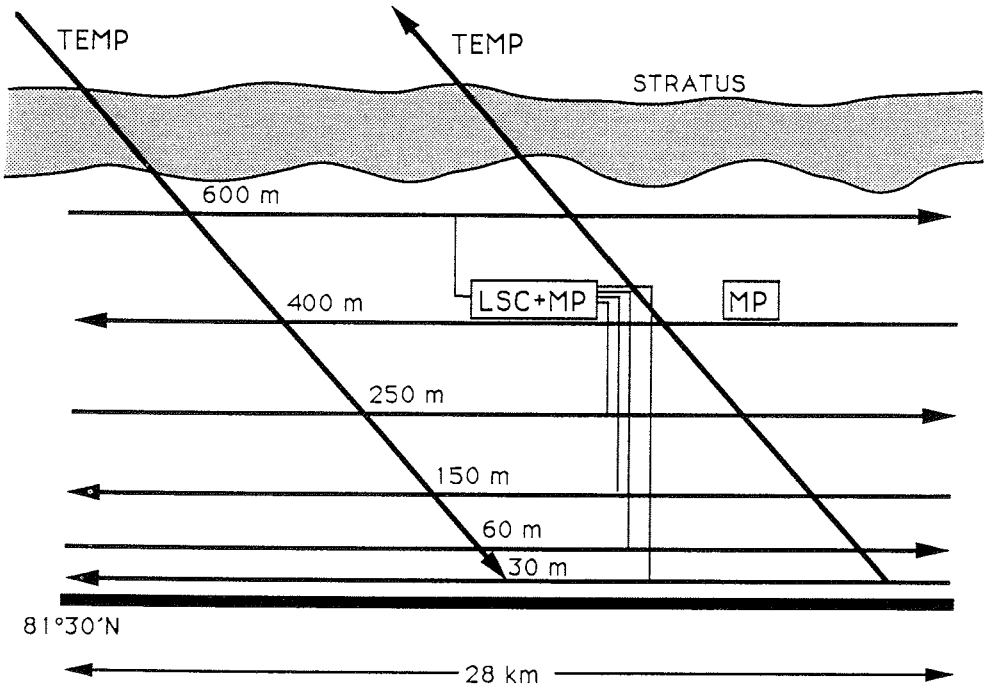

Boundary layer pattern (BLP) : 21 Sept 91

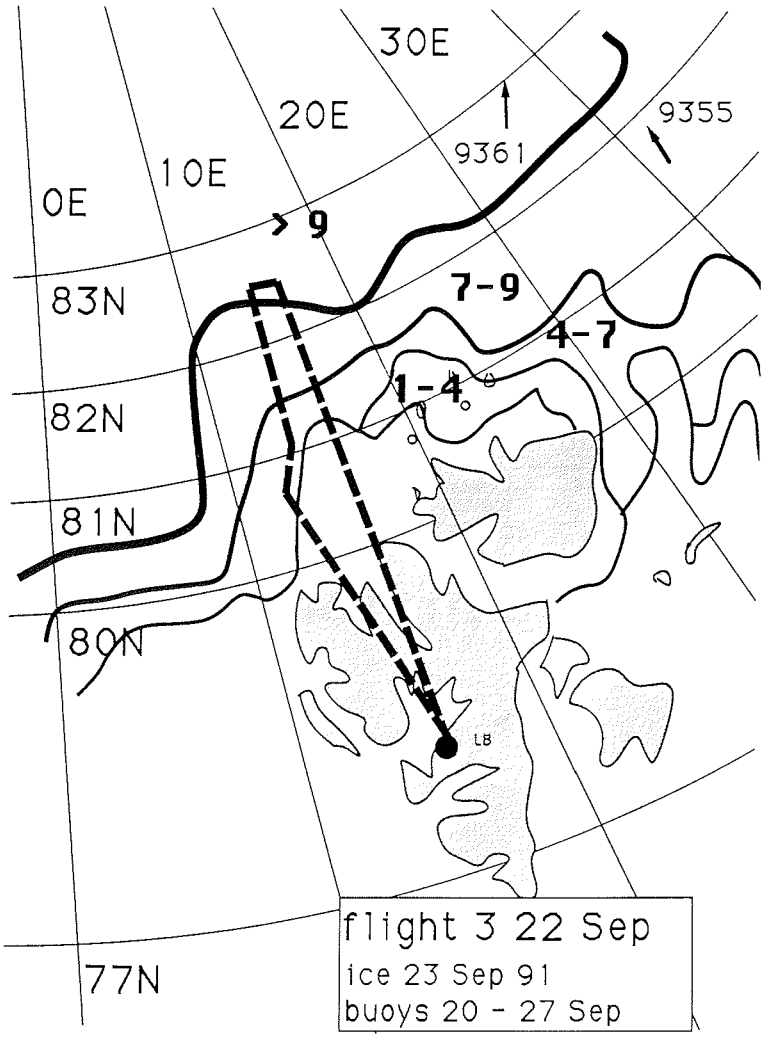

Flight 3, 22 Sep 91, 14:12–16:25

A ridge of a high pressure cell situated northeast of Svalbard extended over the region. Winds were weak from the southeast. Almost cloudless conditions prevailed south of 82°N and fog up to a height of 150 m north of 82°N.

The Line Scan Camera was operated during the northbound leg at an altitude of 3200 m. The return flight was conducted at 30 m about 20 NM east of the north bound track to provide turbulence data upstream of the outbound flight.

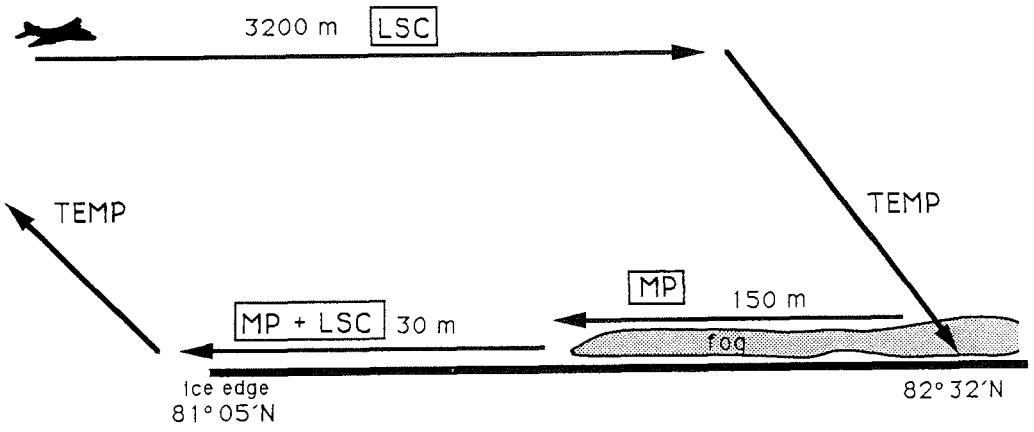

FLIGHT: 22 Sept 91

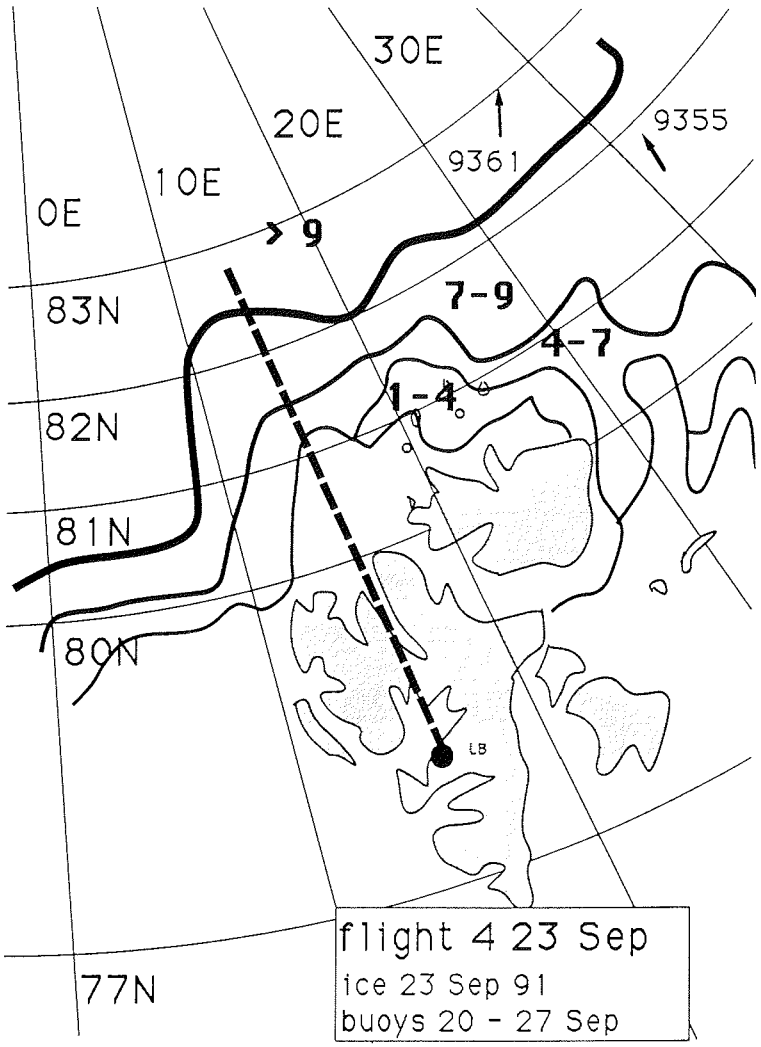

Flight 4, 23 Sep 91, 5:43–8:30

A ridge of a high pressure cell to the northeast of Svalbard extented over the area of operation. Winds were weak from south to southwest. Above a shallow layer of cold air near the ground warmer air with temperatures around 0°C was present. Sea fog forms over open water near the ice margin, a stratus layer from 600 m to 1000 m extends northward of 81°45′N, fog with a top at 150 m is present north of 82°18′N.

The Line Scan Camera was operated during a northbound flight leg at an altitude of 3000 m for a survey of ice conditions, with restrictions due to an intermediate broken cloud deck. A low level flight at a height of 30 m provided turbulence data for the same route. A boundary layer pattern with legs at 3 different heights across the southern fog margin was flown to study the variation of the boundary layer structure.

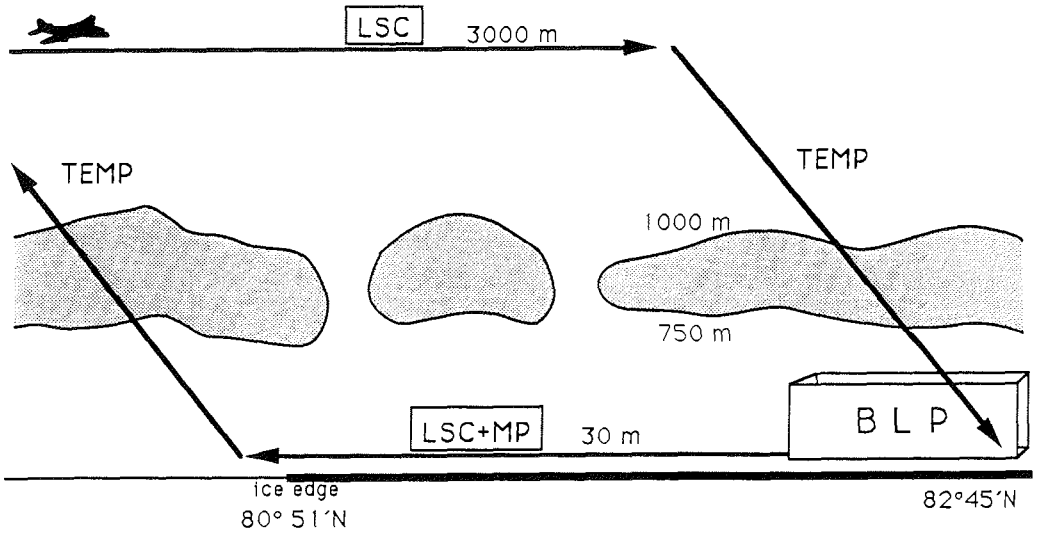

FLIGHT: 23 Sept 91

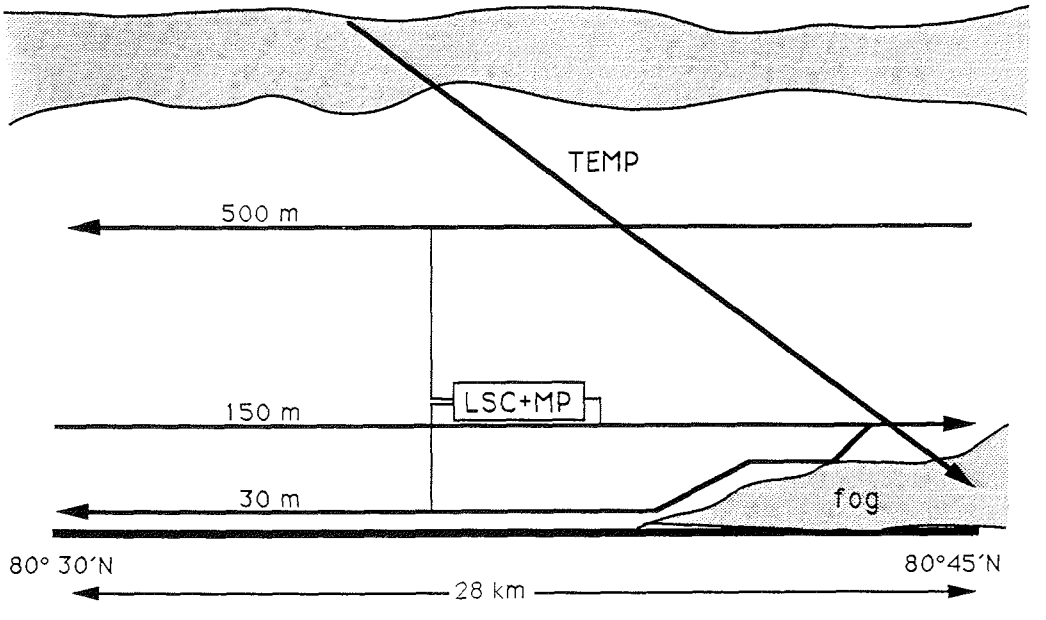

Boundary layer pattern: 23 Sept 91

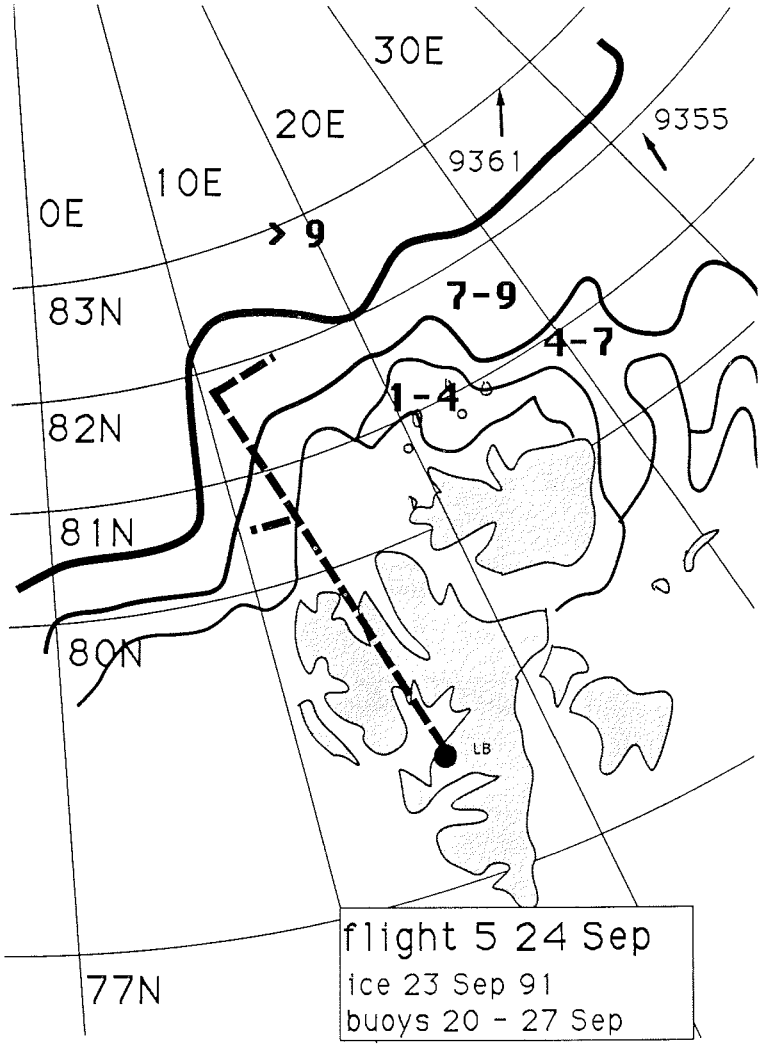

Flight 5, 24 Sep 91, 14:27–16:27

Under the influence of a high pressure cell over Greenland weak southeasterly winds prevailed and several cloud layers existed up to a height of 3000 m. A low stratus cloud layer was present over the sea ice and touched ground a few kilometres north of the ice margin.

The low cloud deck prevented flying in the boundary layer except close to the ice edge. Furthermore, due to a malfunction of the Basic Facility no continuous positioning recording is available. The flight, therefore, was used for extended in-flight calibrations of the Meteopod and other sensors.

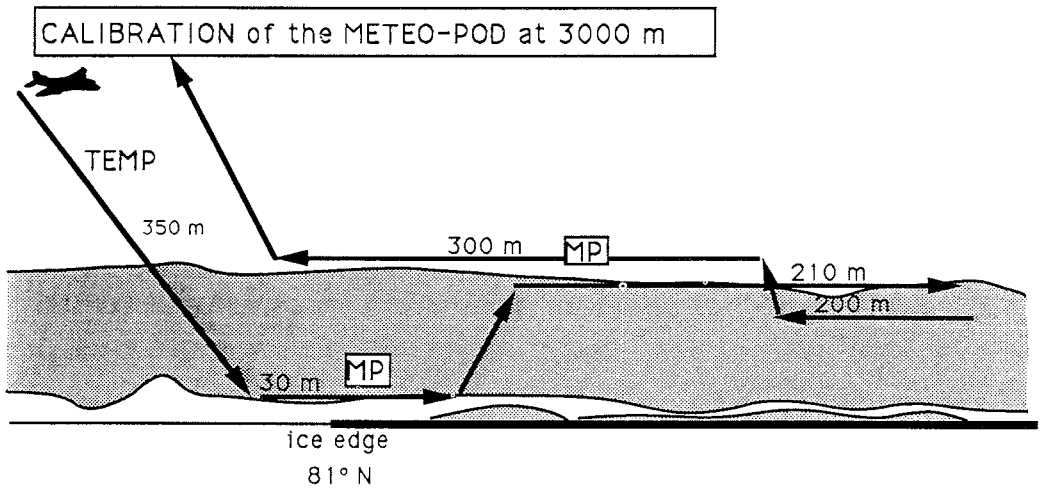

FLIGHT: 24 Sept 91

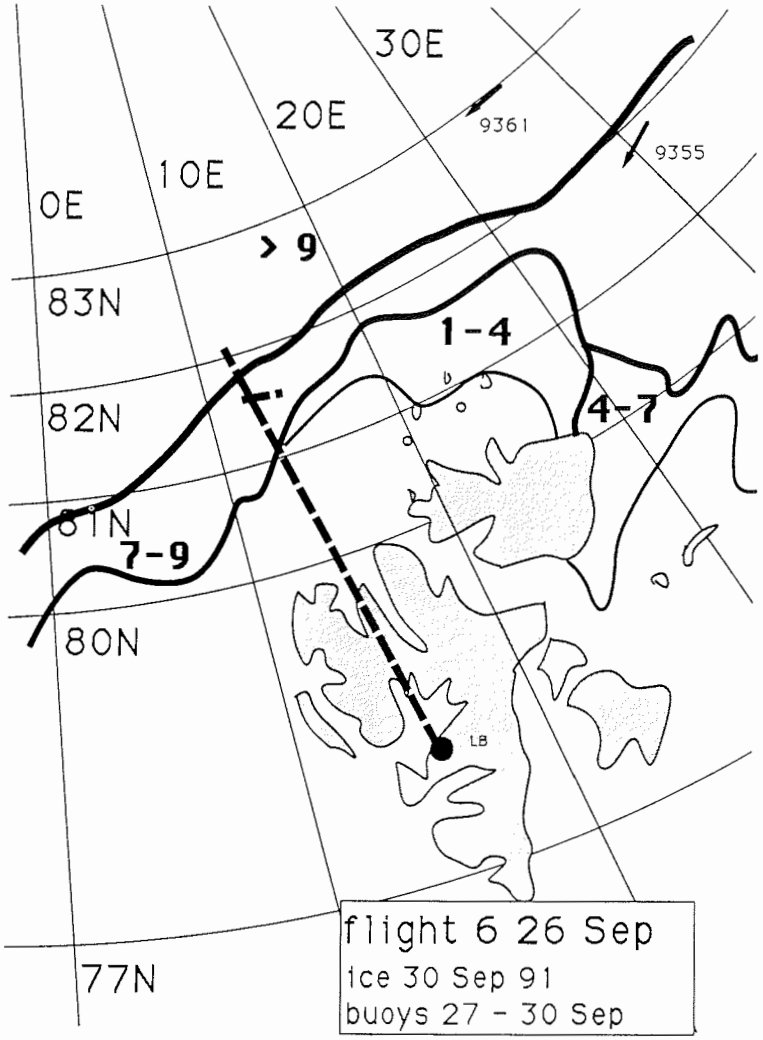

Flight 6, 26 Sep 91, 11:23–13:43

The centre of high pressure was situated over Greenland, affecting off-ice northerly winds in the boundary layer. A low stratus layer was present over the marginal ice zone, but vanished further to the north.

With the onset of an off-ice flow, colder air was advected over the warmer surface. Turbulent fluxes became enhanced in regions of reduced sea ice concentrations and were measured during two low level flights (30 m) across the marginal ice zone. The vertical structure of the atmospheric boundary layer under the presence of broken stratus clouds was observed in the boundary layer pattern at 81°30′N.

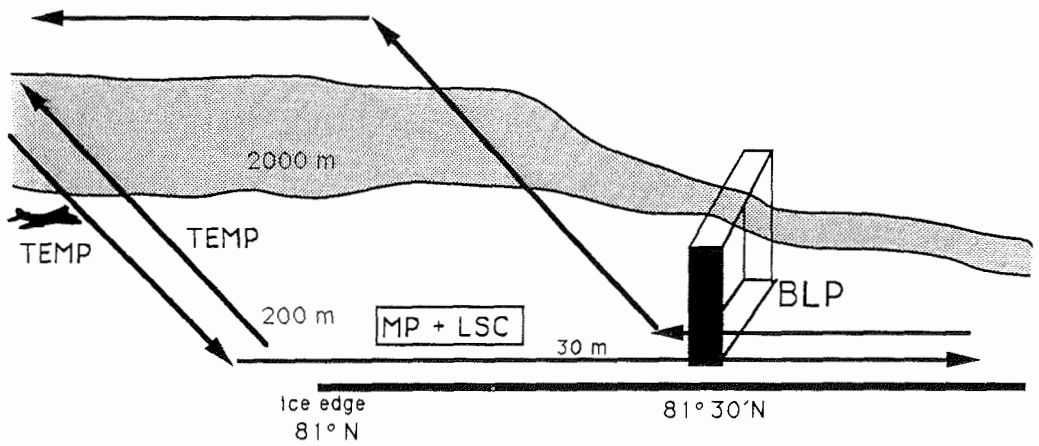

FLIGHT: 26 Sept 91

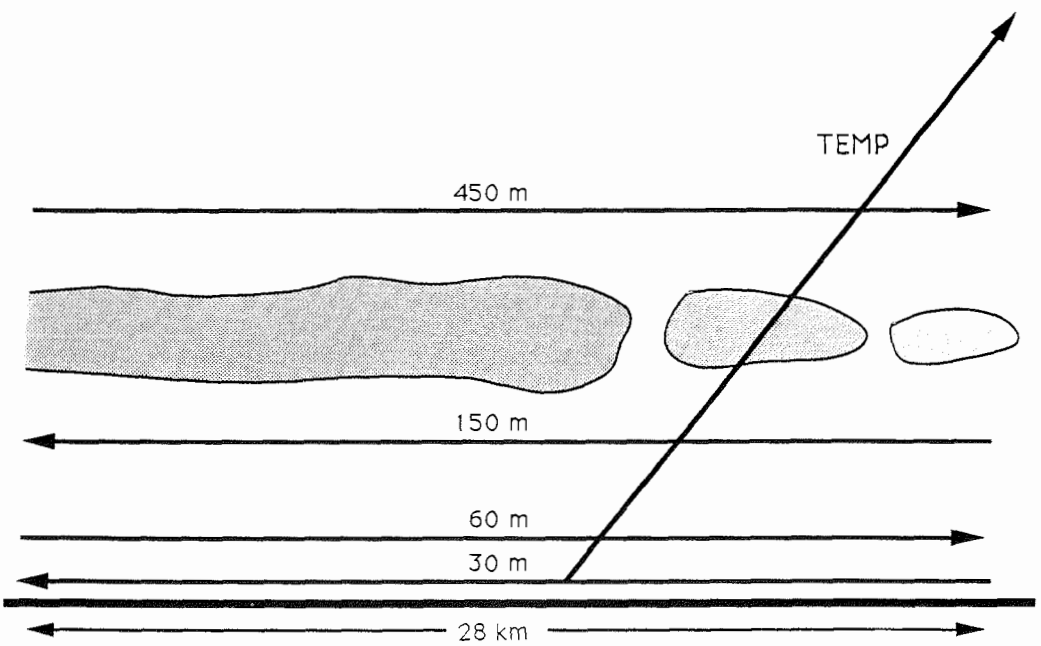

Boundary layer pattern: 26 Sept 91

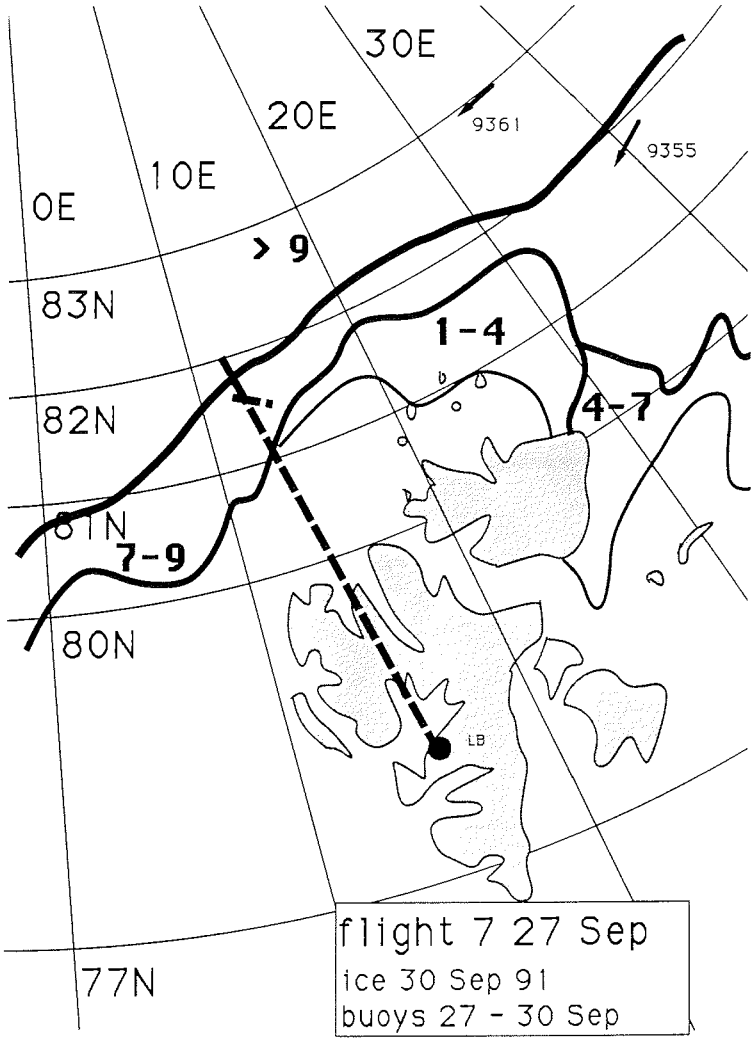

Flight 7, 27 Sep 91, 10:44–14:09

Between a high pressure cell over Greenland and a low pressure system east of Svalbard, cold air moved southward over the sea ice zone. Stratus and altostratus layers in different altitudes extended from 150 m to 3000 m.

Turbulent fluxes and related ice concentrations were measured during low-level flights (30 m and 60 m) between the ice edge and 82°30′N. At 82°30′N a boundary layer pattern was flown, which included 4 legs below the stratus and 2 levels above.

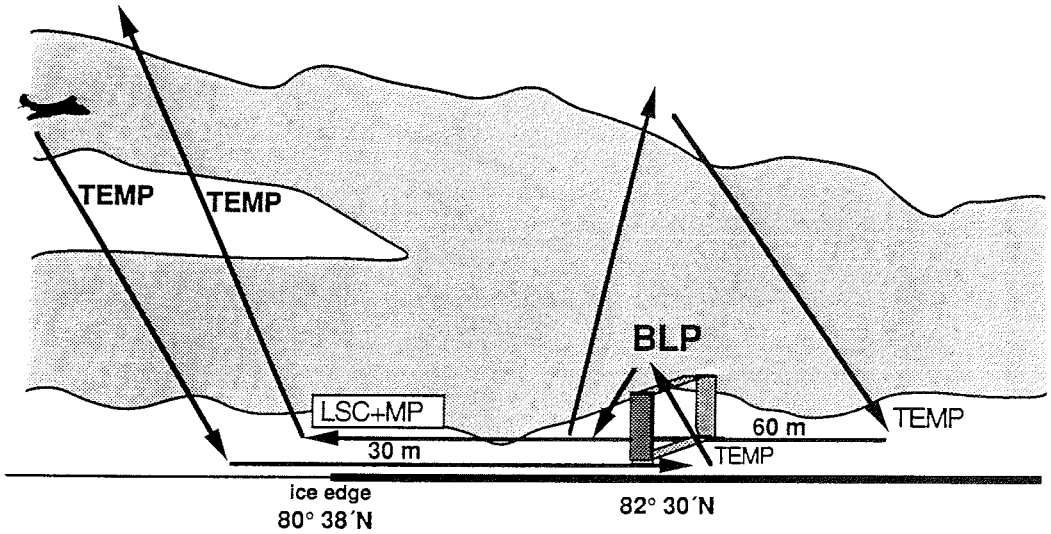

FLIGHT: 27 Sept 91

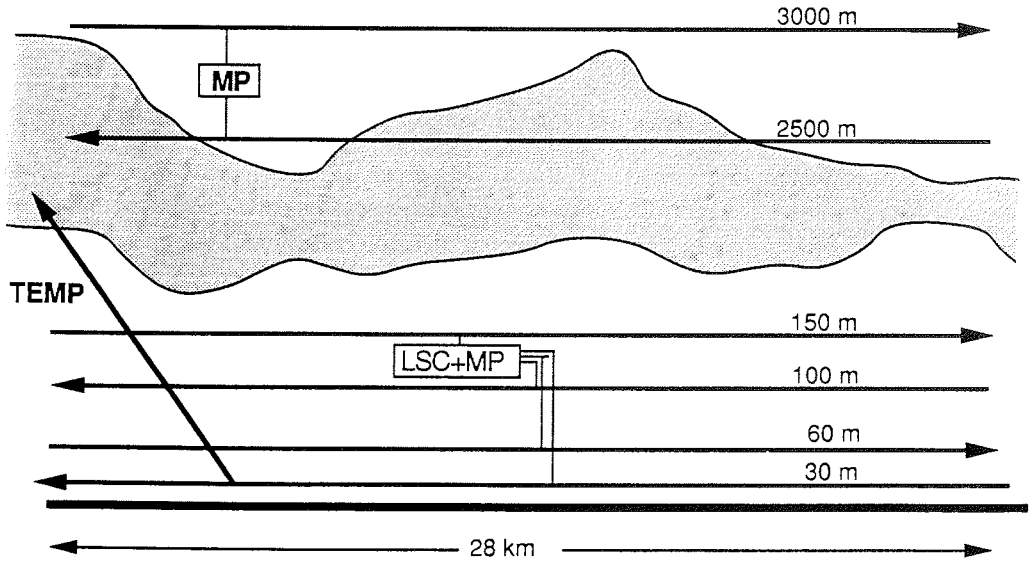

Boundary layer pattern: 27 Sept 91

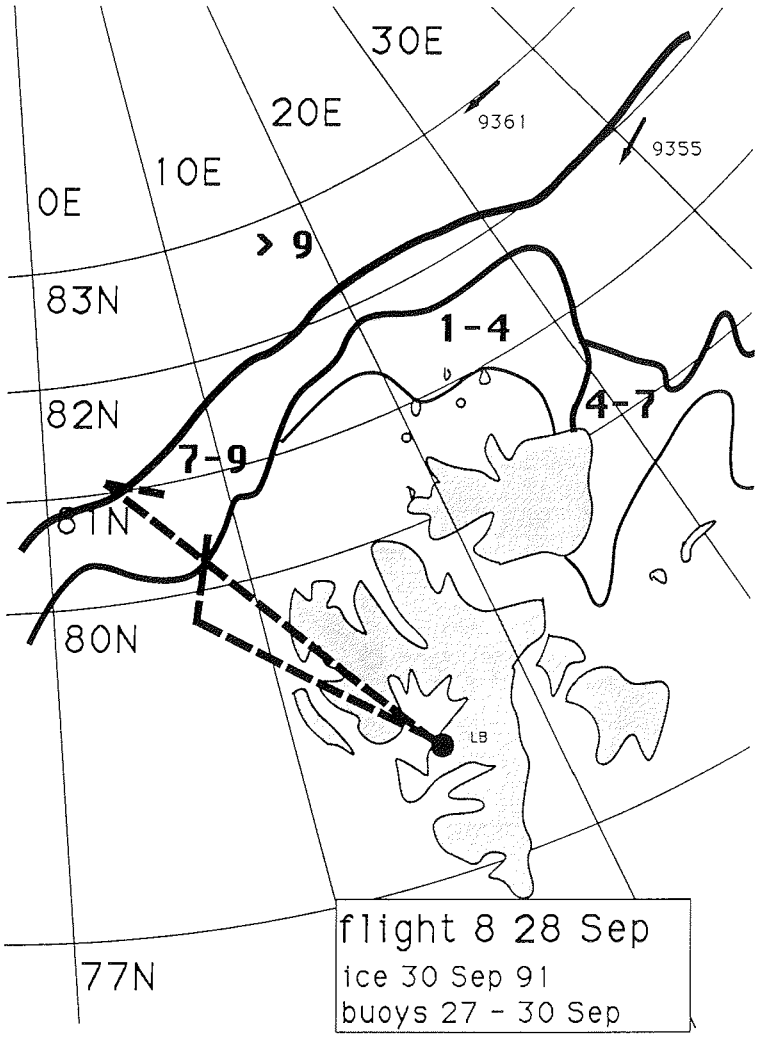

Flight 8, 28 Sep 91, 14:41–17:55

Anticyclonic conditions and a strong north-northeasterly flow prevailed in the area of observation. Variable amounts of stratus clouds in different heights, partly broken, were present over the sea ice. The lowest stratus had tops at 600 m, higher clouds were thin. Downwind of the ice edge sea fog and a thick low stratus layer formed, with raising base due to formation of a convective layer over the water.

The flight consisted of two boundary layer patterns at 81°N and 80°N and low-level legs between them. The latter were extended over the open water south of the ice edge. Turbulent fluxes increased with decreasing ice concentration, especially in the convective layer over the open water.

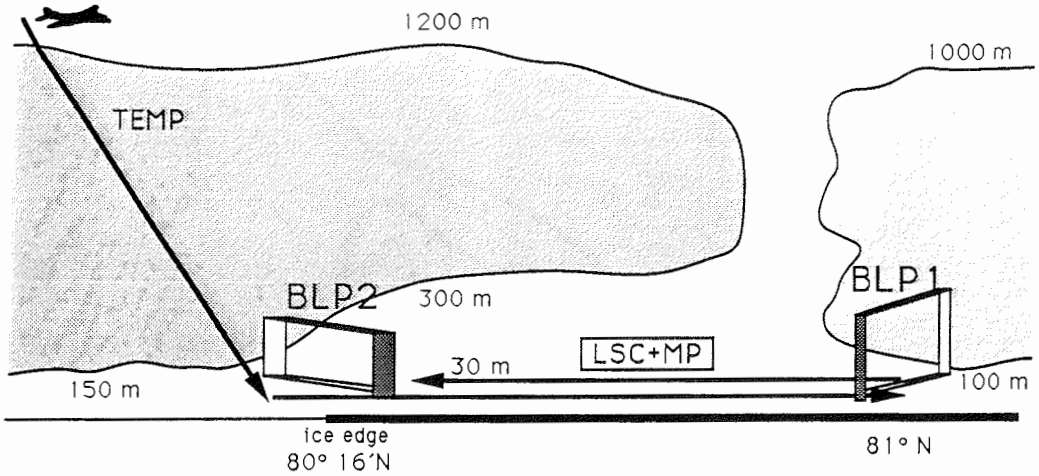

FLIGHT: 28 Sept 91

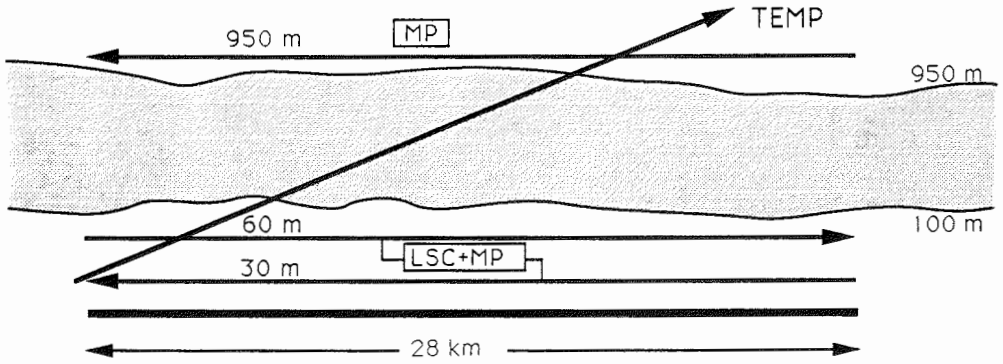

Boundary layer pattern1: 28 Sept 91

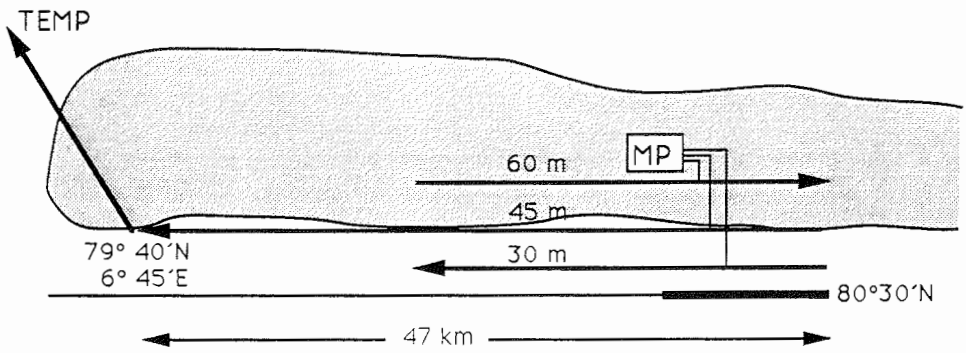

Boundary layer pattern 2: 28 Sept 91

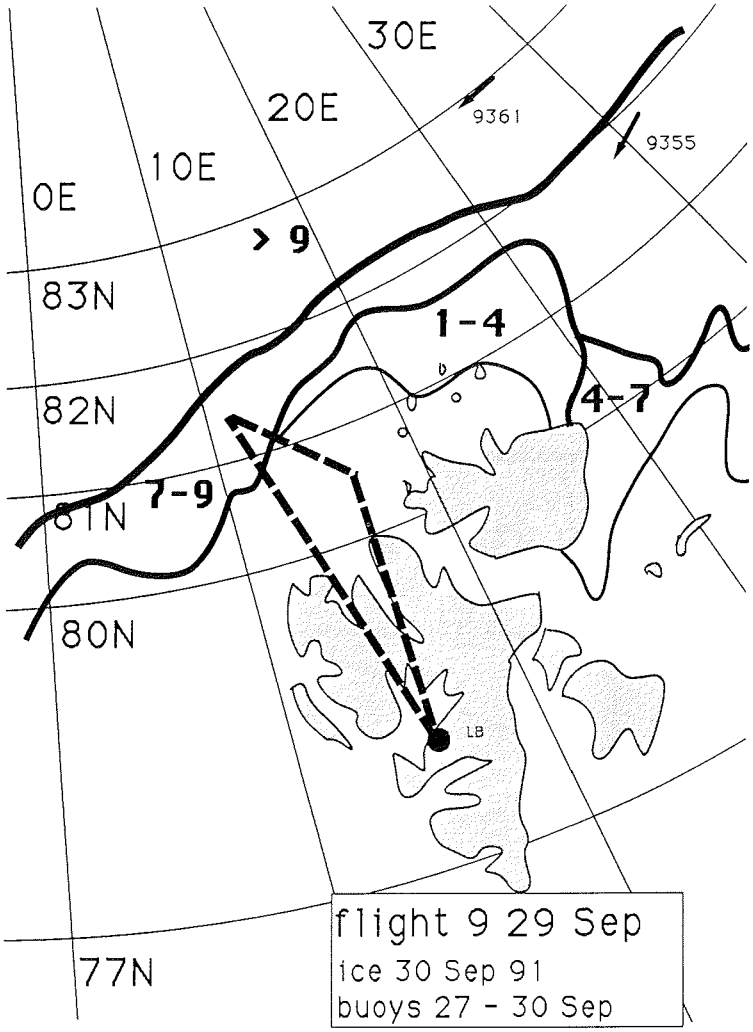

Flight 9, 29 Sep 91, 13:34–16:38

A ridge of the high pressure cell over Greenland extended in the marginal ice zone north of Svalbard. Winds were northeasterly and strong. Cloudless conditions prevailed over the sea ice. Roll type low stratus clouds developed downwind of the ice edge and gradually changed into an overcast stratus layer.

Three runs at heights of 30 m, 60 m and 150 m were flown between 80°30′N and 81°20′N. About 1/3 of their lengths were above sea ice and 2/3 in the convective layer over open water. Intense low level turbulence and roll type convection with significant downwind modification was observed over open water.

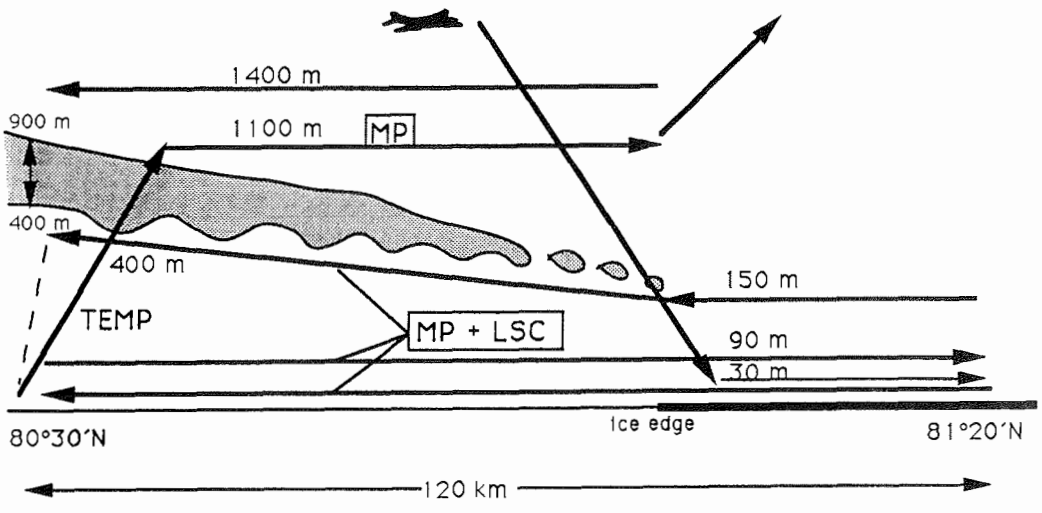

FLIGHT (BLP): 29 Sept 91

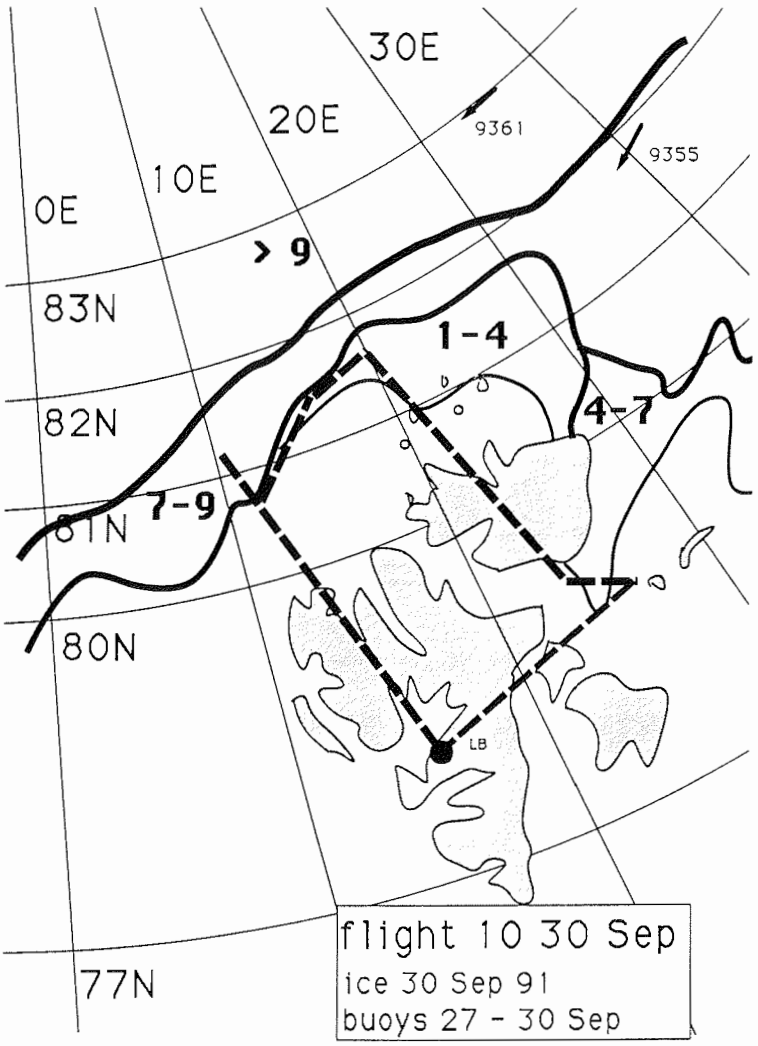

Flight 10, 30 Sep 91, 12:00–15:02

Under anticyclonic conditions a weak northeasterly flow prevailed. Low stratus clouds were present both above sea ice and open water. Occasionally light snow fall and icing beneath and within the clouds was observed.

Due to reduced visibility and icing on the instruments the flight could only be used for a general survey of the ice extent in the region to the north and east of Svalbard.

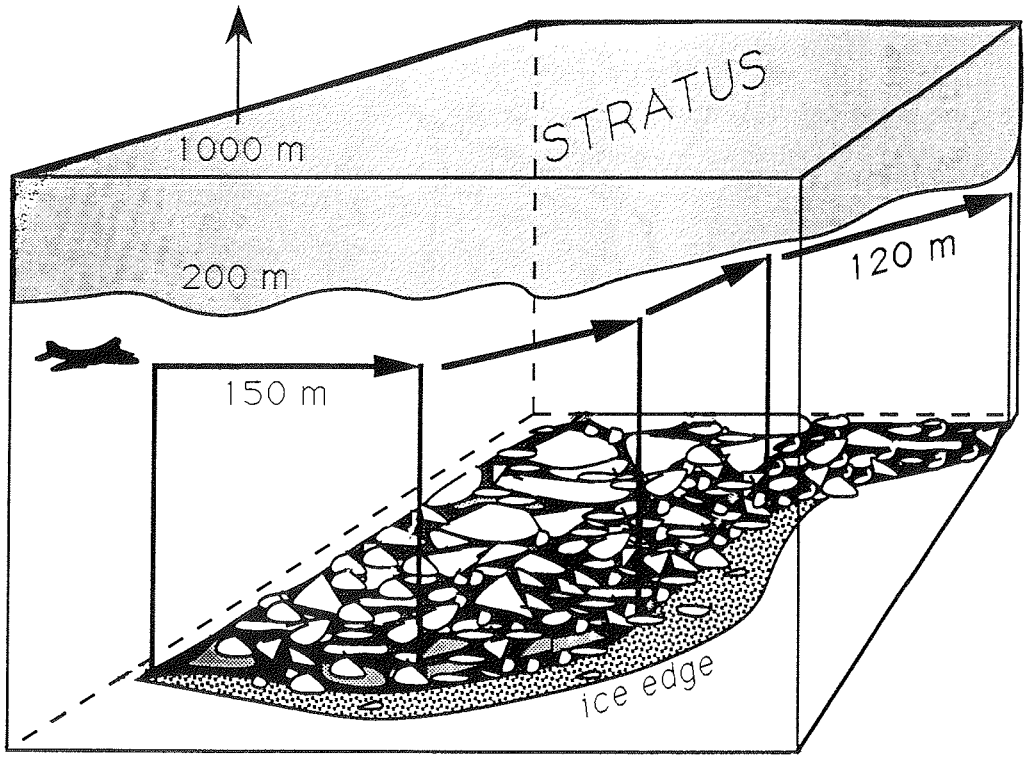

Ice edge reconnaissance flight:30 Sept 91

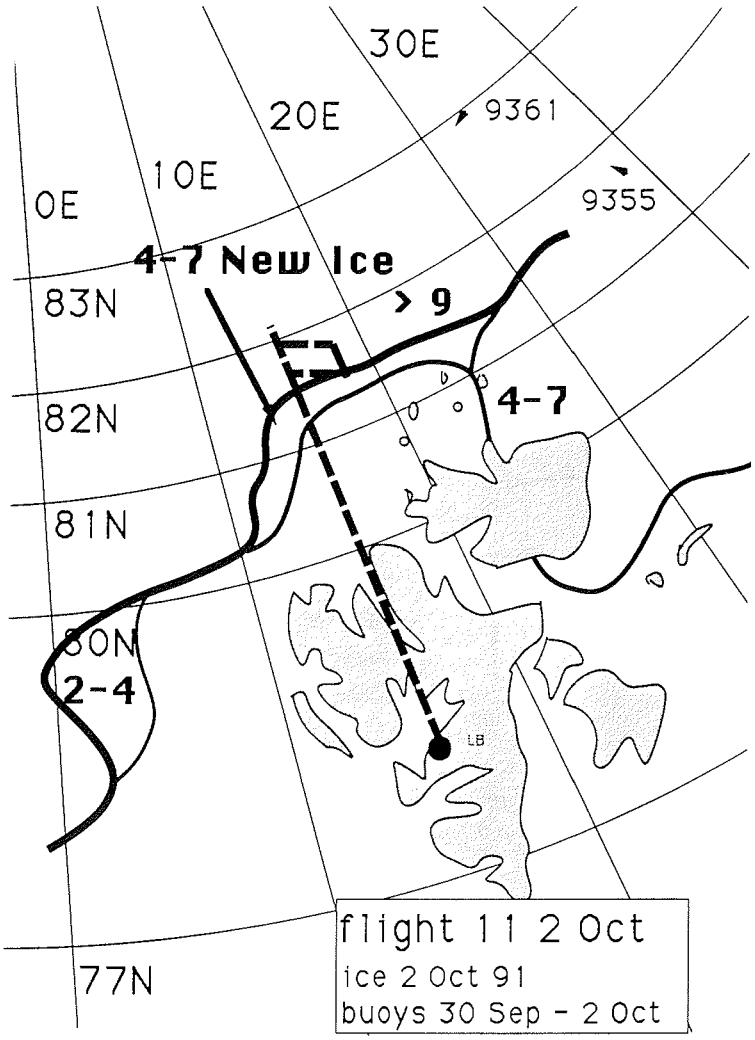

Flight 11, 02 Oct 91, 12:01–14:37

The area of observation was influenced by the Greenland anticyclone with moderate winds from NNE advecting cold air towards the ice edge. Low stratus clouds were present south of the border between old ice and young ice. The stratus extended over open water, where both thickness and base height increased with distance from the ice edge. No clouds were observed over the old ice.

Based on two boundary layer patterns the state of the atmospheric boundary layer was observed under conditions of slightly unstable thermal stratification over the sea ice. A low level run (90 m) extended to 82°N.

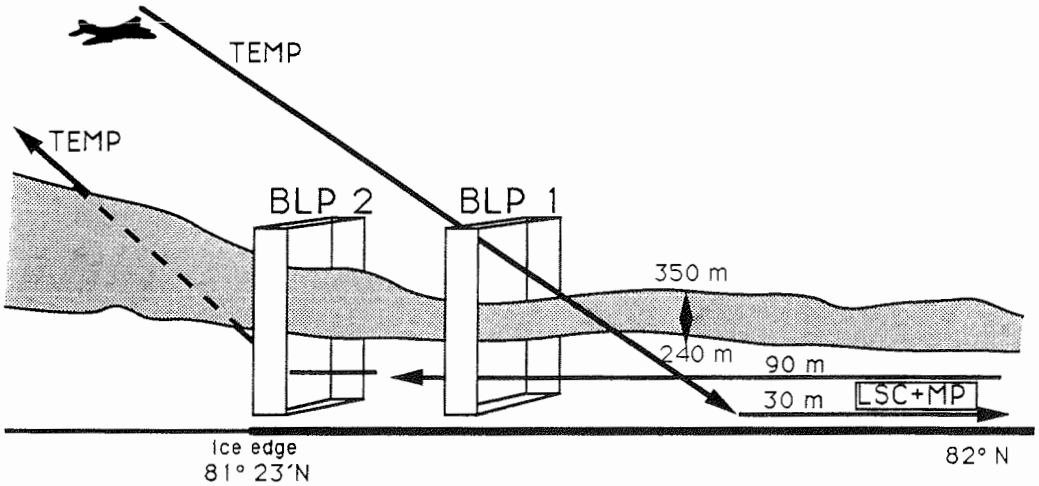

FLIGHT: 2 Oct 91

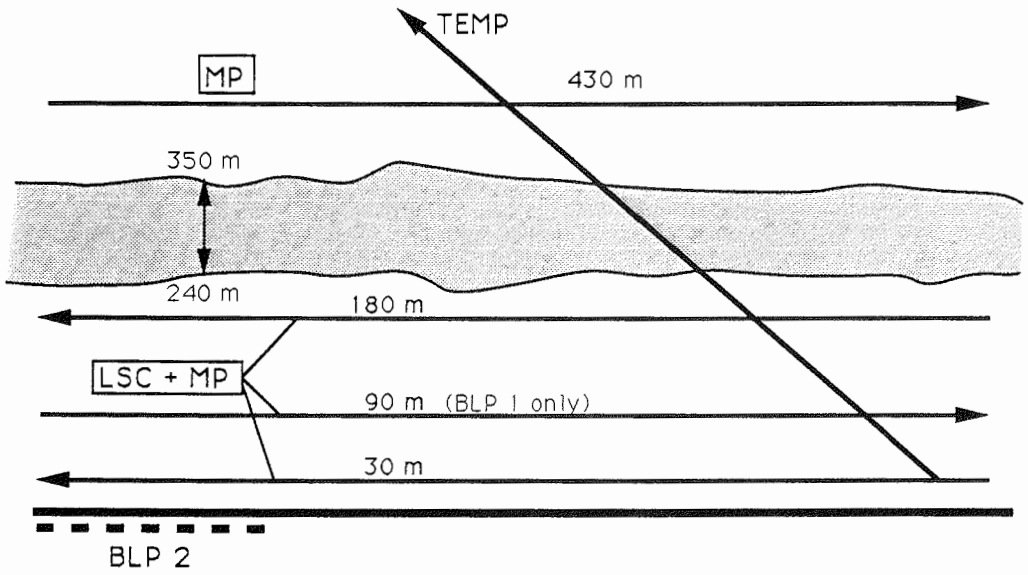

Boundary layer patterns 1,2: 02 Oct 91

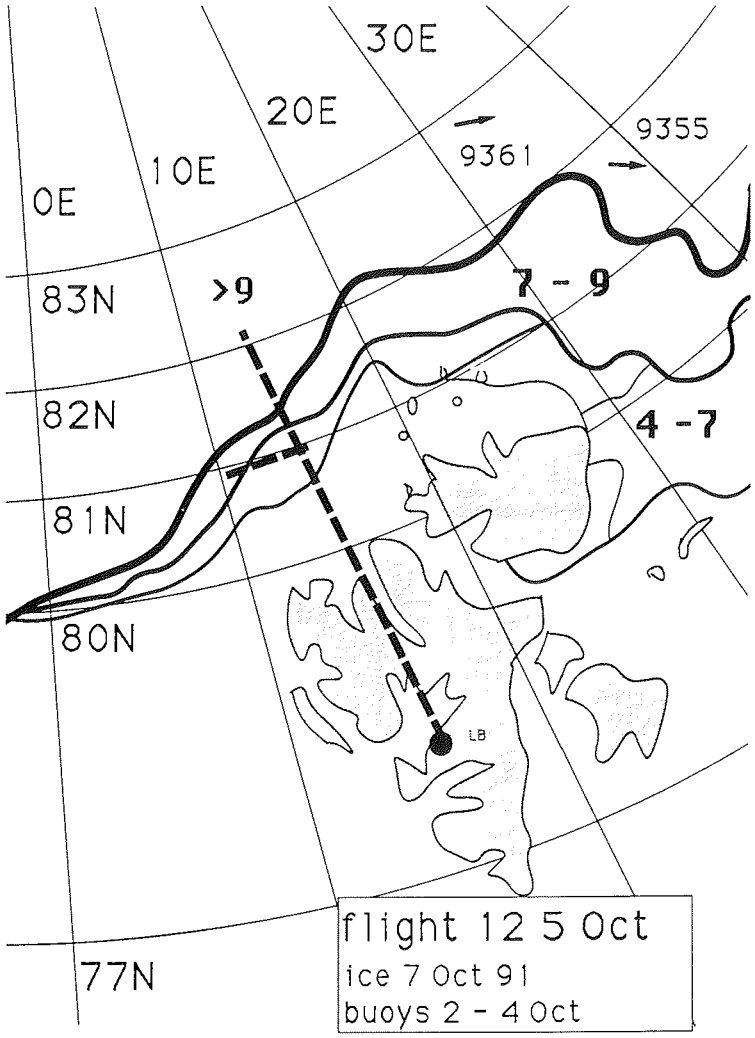

Flight 12, 05 Oct 91, 13:01–15:52

Under anticyclonic conditions winds in the marginal ice zone were weak. Wind directions were from NW to N near the ice edge and from NE at 81°N. No clouds were observed south of 82°N, stratus and fog occurred north of 82°N.

The flight combined a high level leg (2100 m) for LSC observations to 82°N with a low level flight (30 m) back. Over new sea ice which developed during the previous days close to the ice edge, a boundary layer pattern was flown to study turbulent fluxes over thin ice.

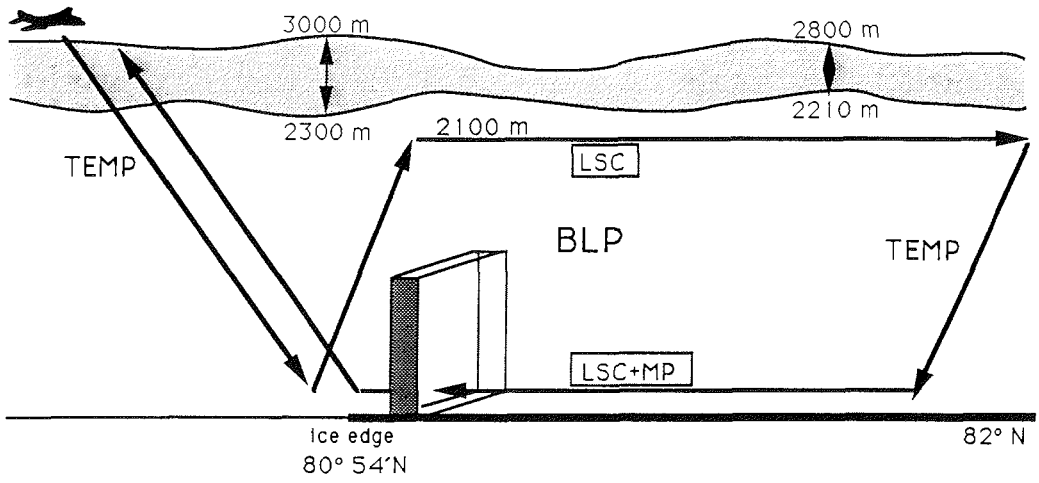

FLIGHT: 05 Oct 91

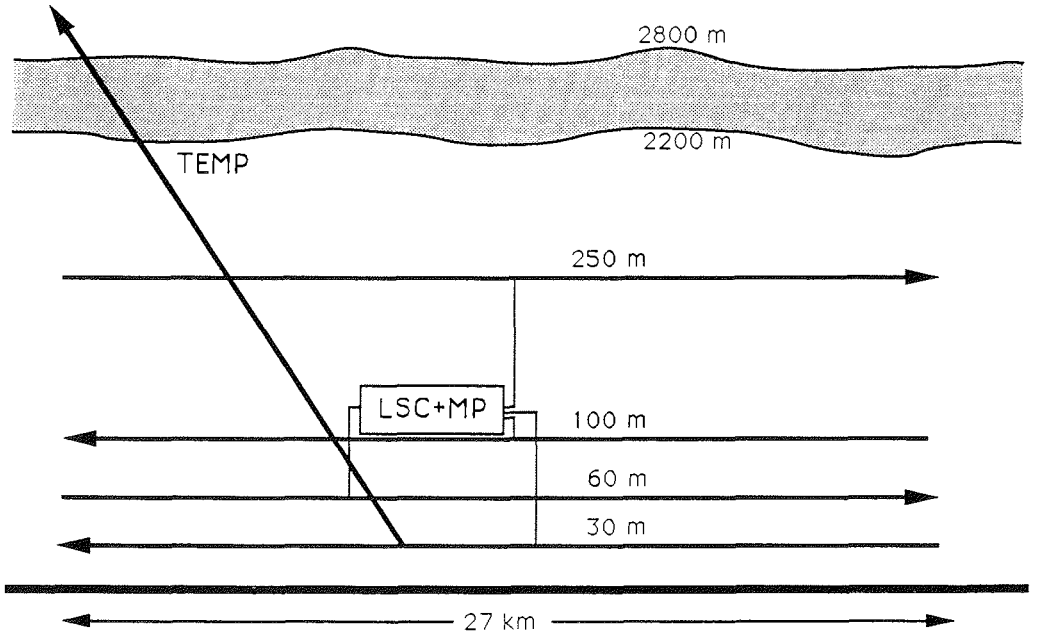

Boundary layer pattern: 05 Oct 91

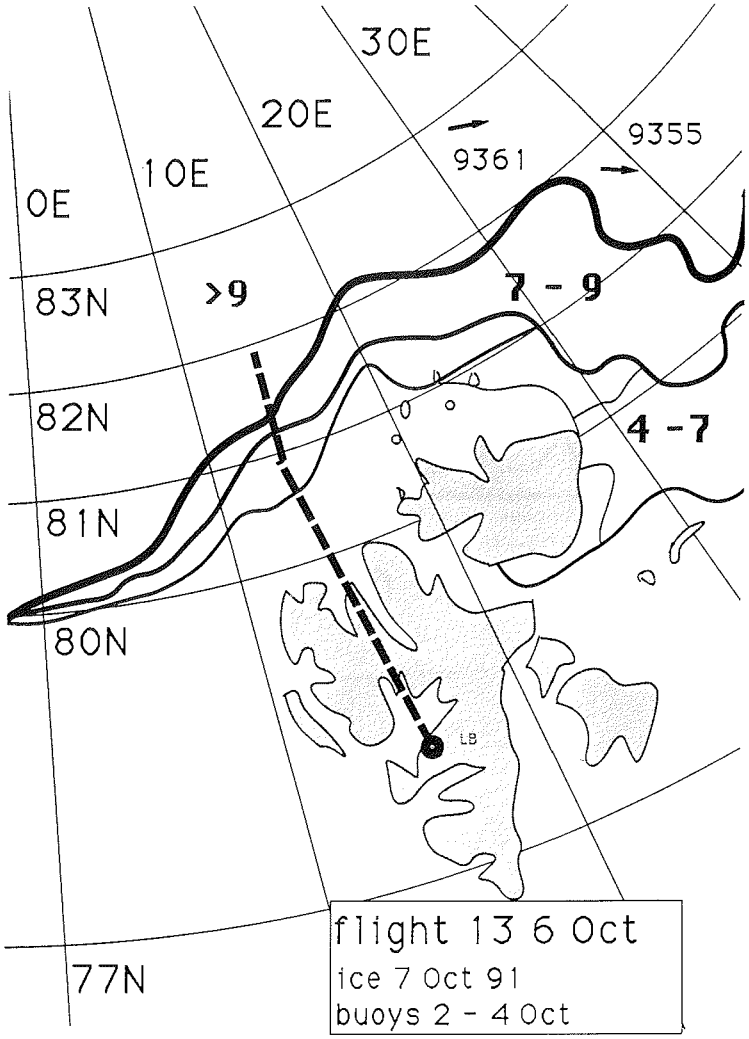

Flight 13, 06 Oct 91, 12:41–14:32

In an anticyclonic situation with weak pressure gradients a warm southerly flow entered the sea ice region. An 8/8 stratus layer extended north of Svalbard. North of the ice edge the base of the stratus lowered and reached the surface.

A boundary layer pattern was flown near the ice edge, where the cloud base was sufficiently high. It extended from the ice edge over thin new ice and young ice.

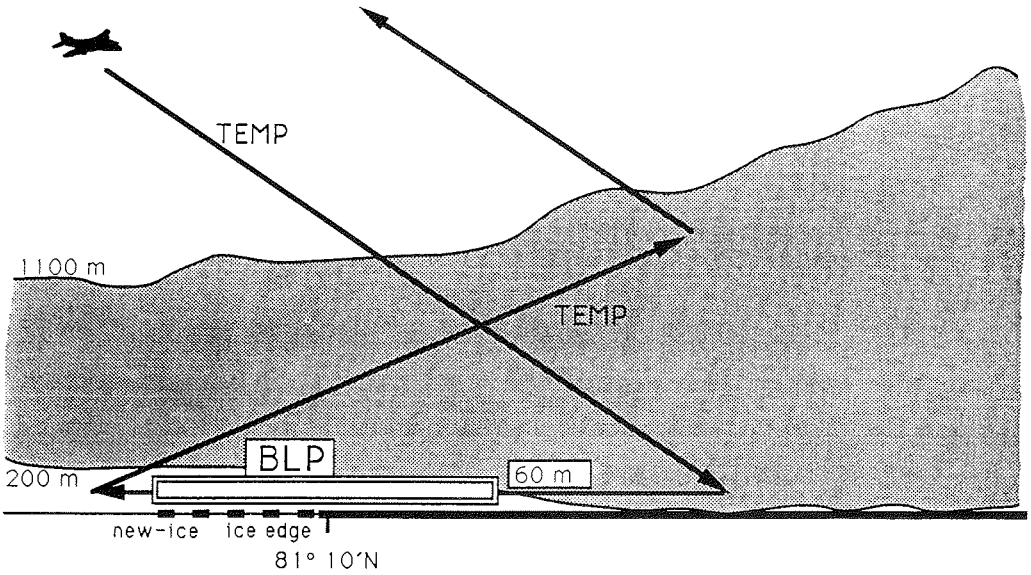

FLIGHT: 06 Oct 91

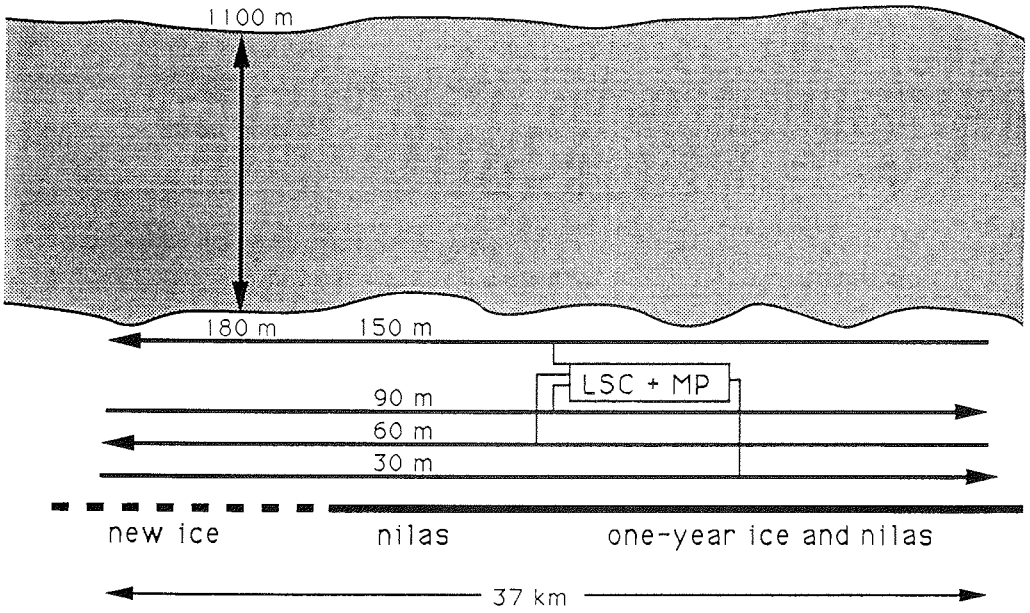

Boundary layer pattern: 06 Oct 91

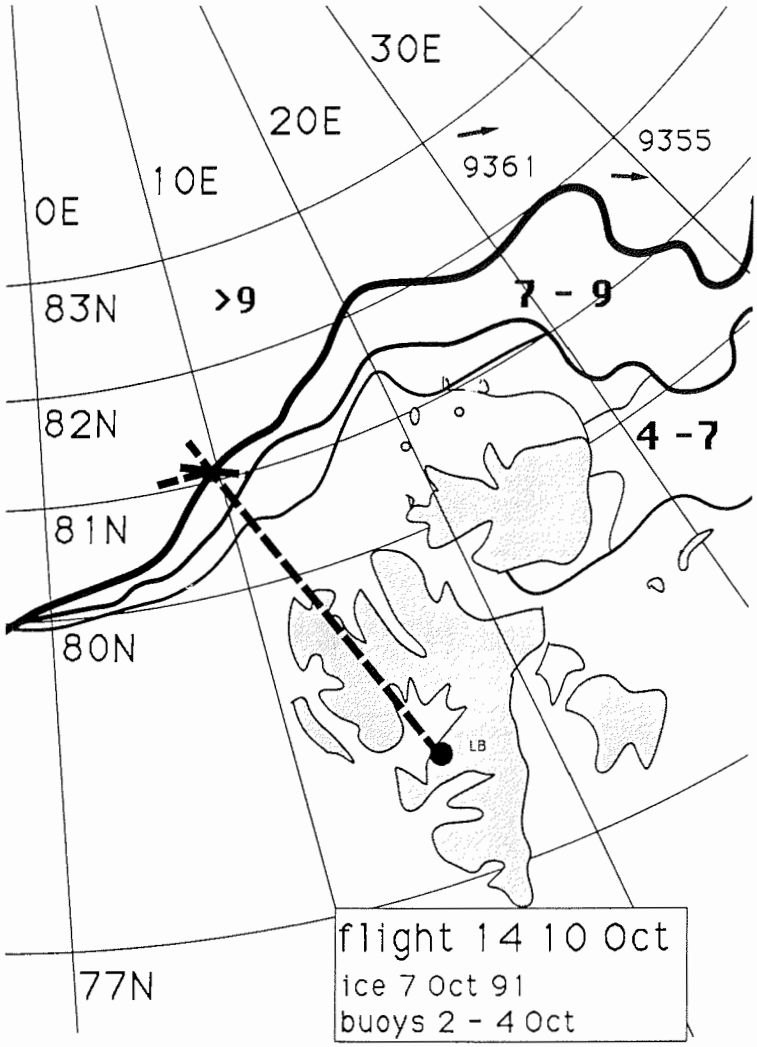

Flight 14, 10 Oct 91, 11:07–13:44

Between low pressure systems to the east and southwest of Svalbard a weak high pressure ridge caused moderate southeasterly winds near the ice edge and northeasterly winds at 81°N. A stratus layer extended from the open water to 81°N, where it became translucent. Further to the north the cloud cover decreased. Temperatures dropped significantly with increasing distance from the ice edge.

The flight was performed to study boundary layer turbulence and radiation fluxes above sea ice of different characteristics in the presence of overcast stratus clouds. A low level flight started south of the ice edge and extended to 81°20′N. Two boundary layer patterns were flown at 81°N.

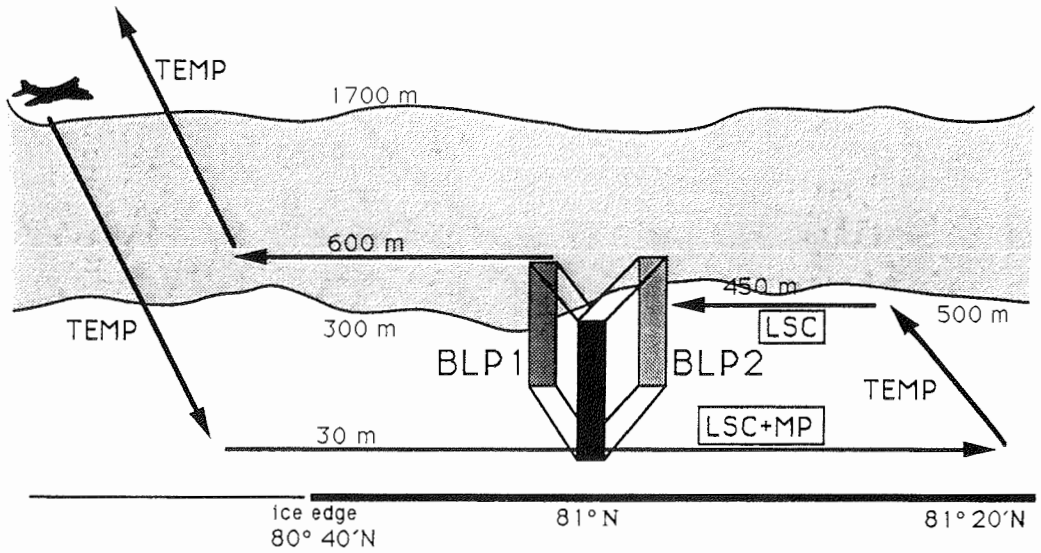

FLIGHT:10 Oct 91

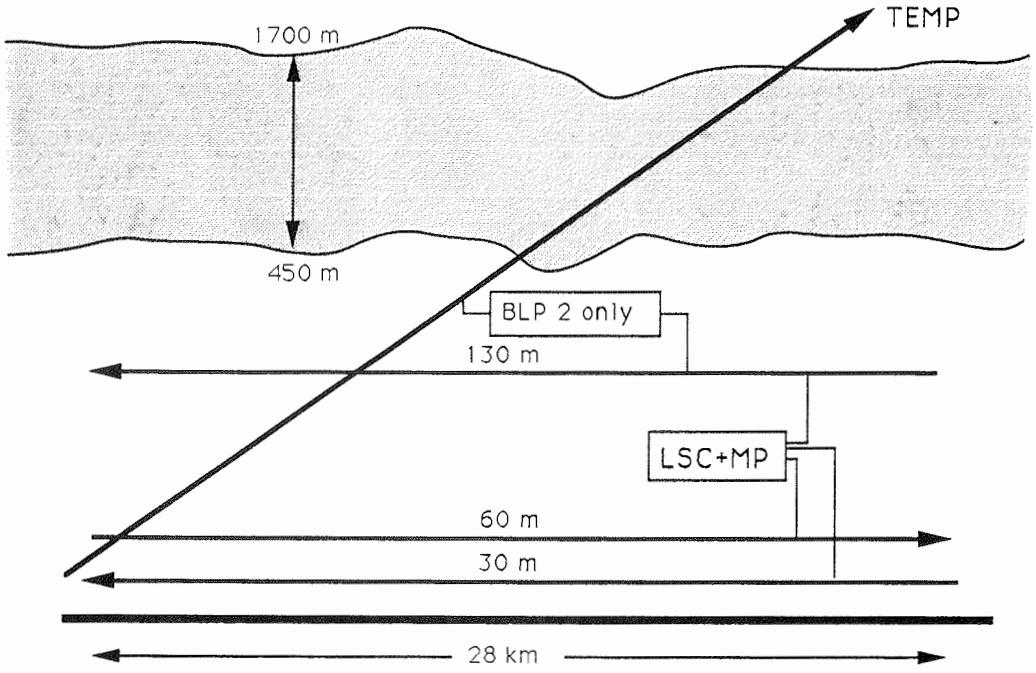

Boundary layer patterns 1,2:10 Oct 91

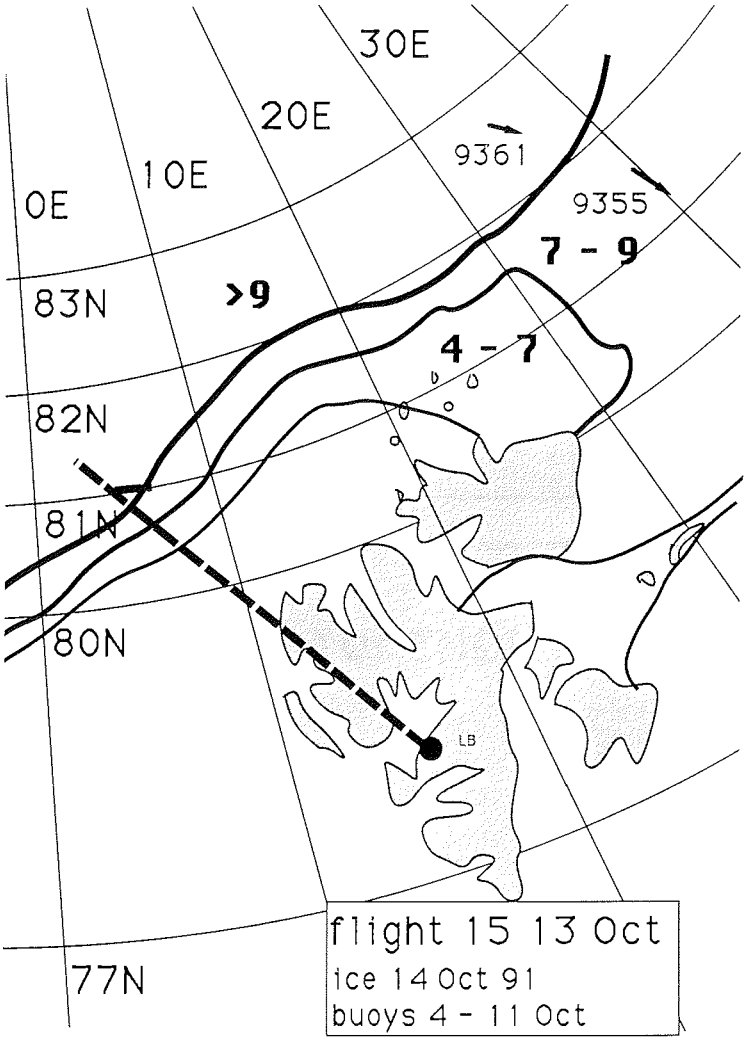

Flight 15, 13 Oct 91, 12:06–14:52

A low pressure system with scattered snowfall was centered over the south of Svalbard. A high pressure ridge approached the marginal ice zone. Winds turned to a northerly direction. A closed layer of stratus clouds was present over the sea ice with cloud bases at 1000 m and cloud tops at 1300 m above ground. Over the open water the stratus increased in thickness and reached ground.

Two boundary layer patterns were flown over the open water close to the ice edge and 110 km north of it, respectively, to study the modifications of the turbulent fluxes and of the boundary layer structure due to heating from below.

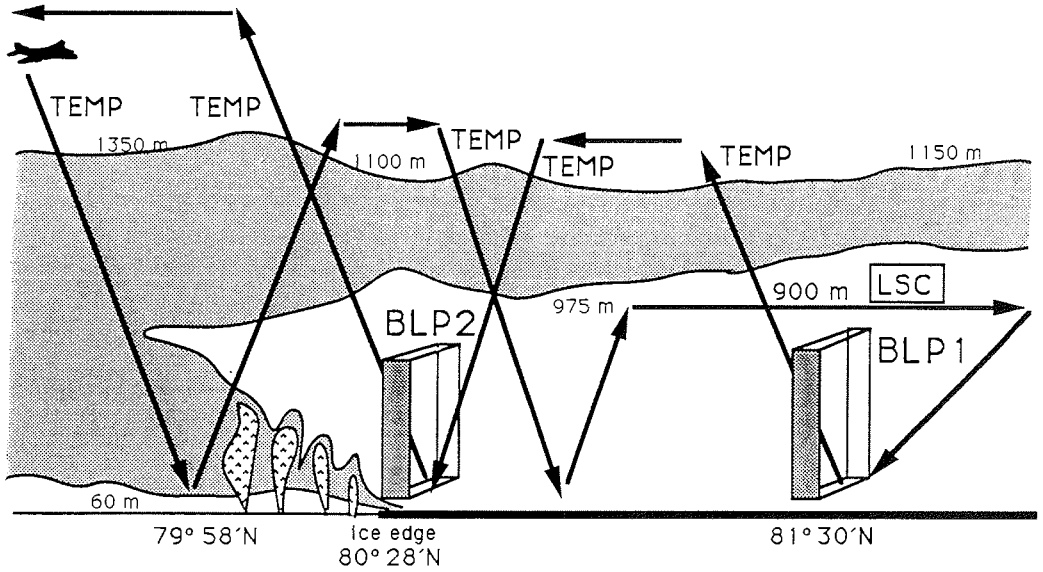

FLIGHT: 13 Oct 91

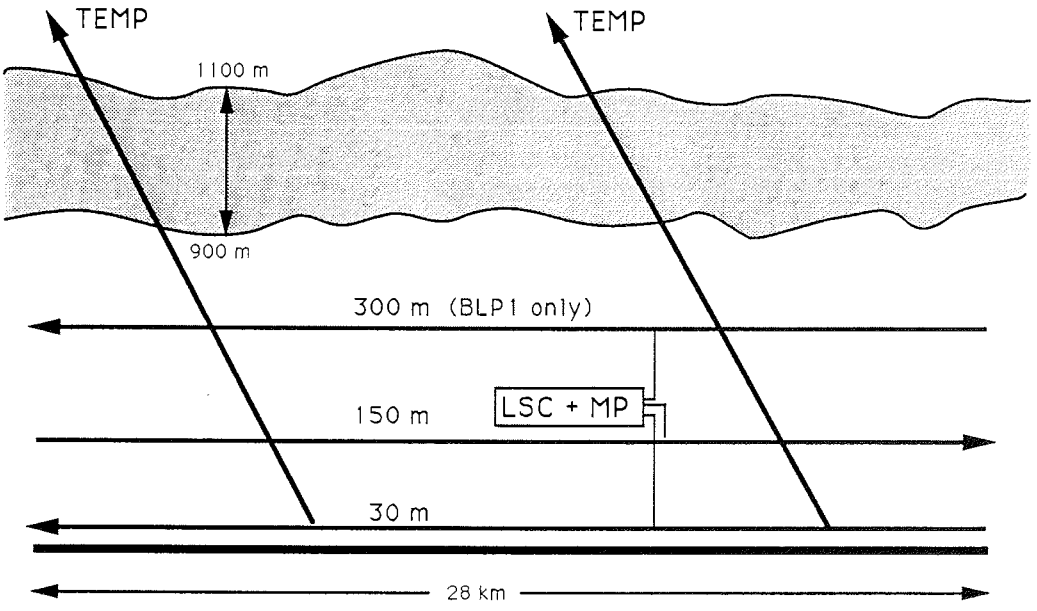

Boundary layer patterns 1,2 : 13 Oct 91

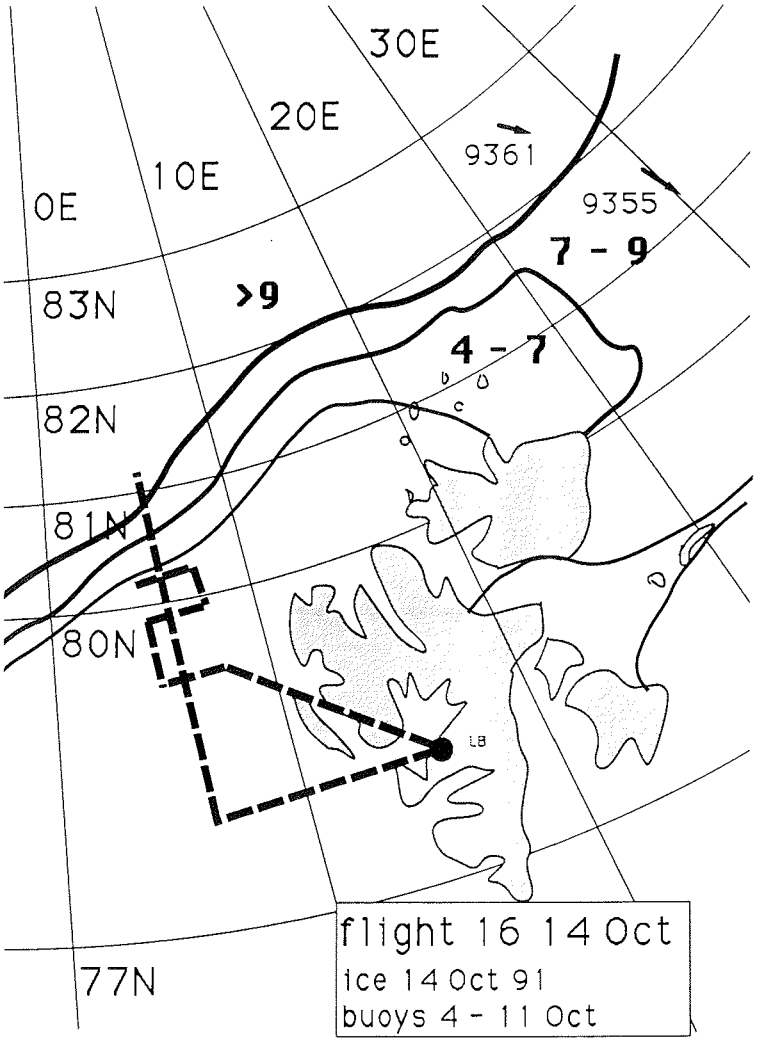

Flight 16, 14 Oct 91, 13:53–14:30

A weak depression over southern Svalbard moved southward. High pressure prevailed north of 78°N. Winds in the boundary layer were fresh from the north and remained constant with height. Air temperatures above the ice were at −18°C. The ice zone was free of clouds, a stratocumulus layer developed south of the ice edge and thickened with increasing fetch over water.

The evolution of the atmospheric boundary layer downstream of the ice edge was investigated by means of aerological sondes dropped from *Polar 2* during the northward approach to the ice. Ice concentrations with LSC and turbulence data were obtained within the first 60 km of the ice zone. In the intensely convective layer south of the ice edge 3 cross wind legs were flown at different distances from the ice edge in order to derive the structure of the convective elements.

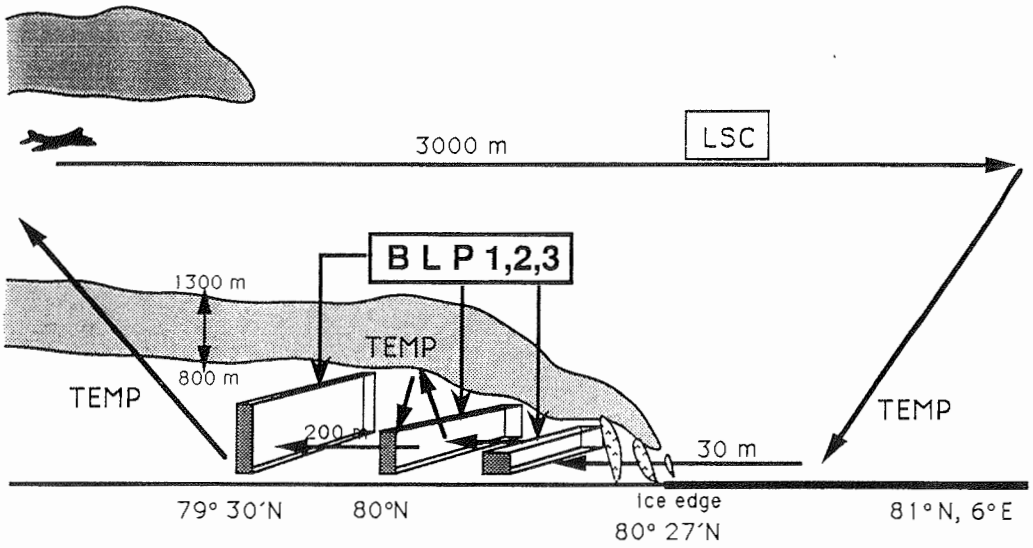

FLIGHT:14 Oct 91

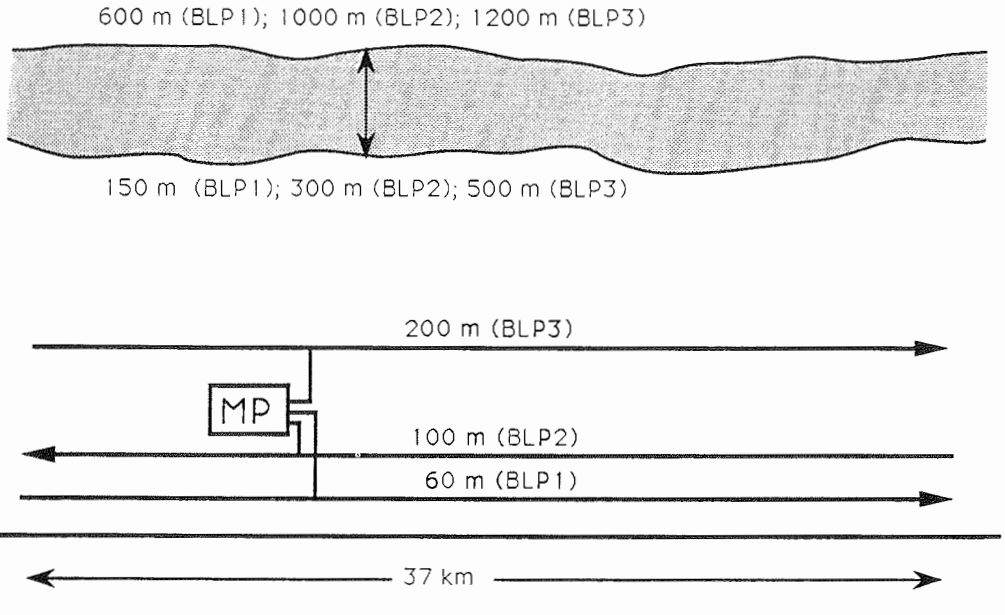

Boundary layer patterns: 14 Oct 91

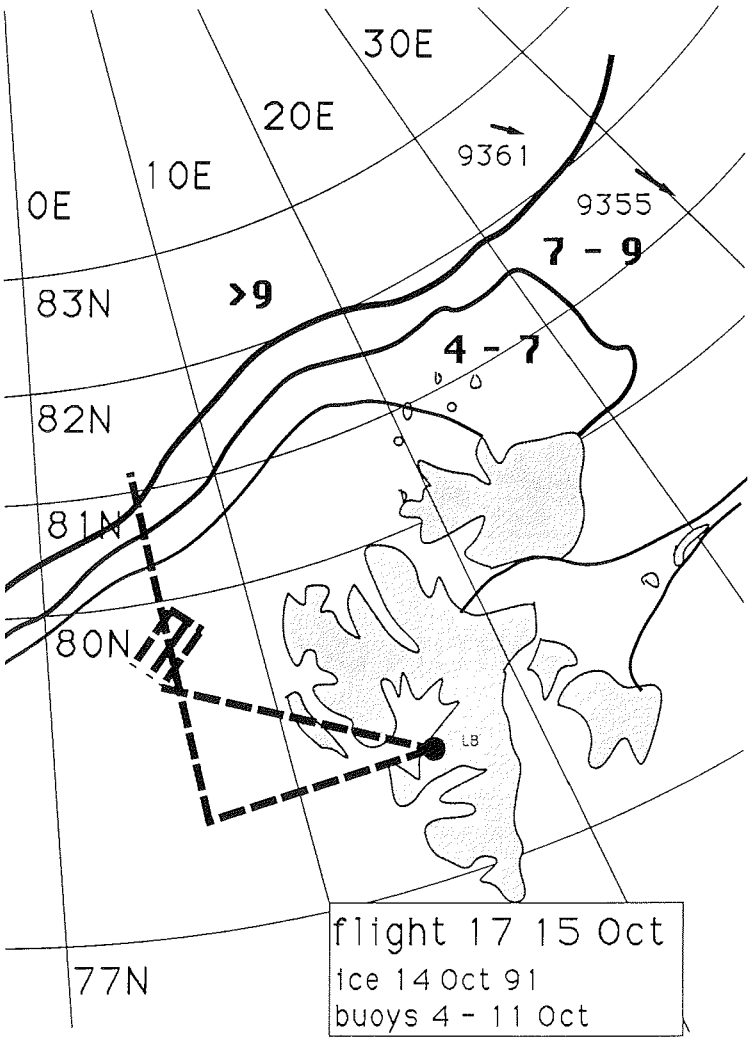

Flight 17, 15 Oct 91, 12:43–14:33

Under anticyclonic conditions a northwesterly flow advected cold air from the sea ice over the open water. No clouds were present over the ice. A stratocumulus layer developed over the ocean. Cloud bases and thickness increased with increasing fetch. Light snowfall occurred around 40 km off the ice edge.

A flight similar to the day before was flown. Dropsondes were released from 3000 m height on the long northbound approach to the ice edge and a few tens of kilometres into the ice. LSC and turbulence measurements were made on a low-level flight back to the ice edge. Over water 3 cross-wind runs were flown to measure the structure of convection.

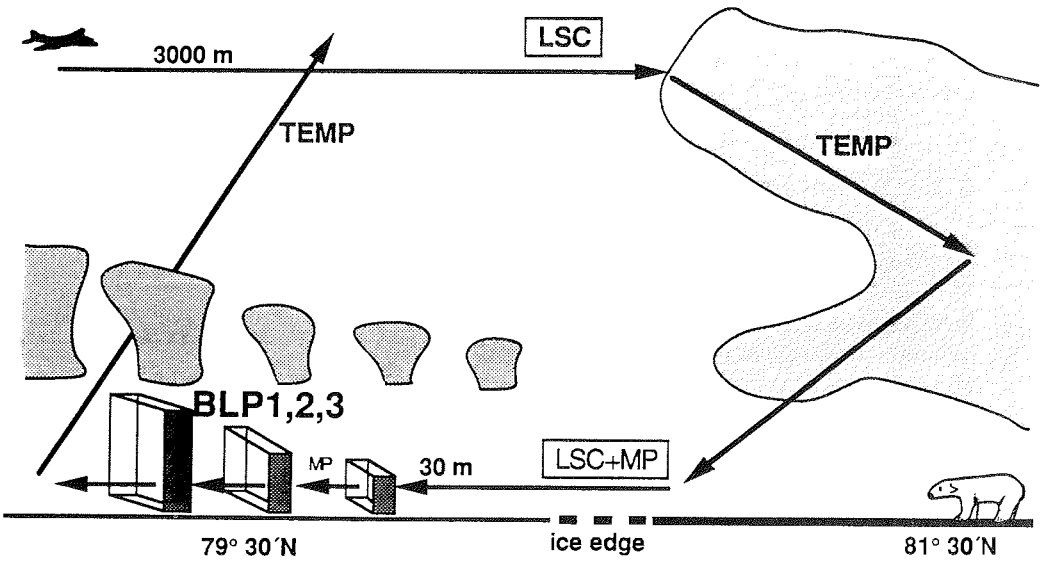

FLIGHT: 15 Oct 91

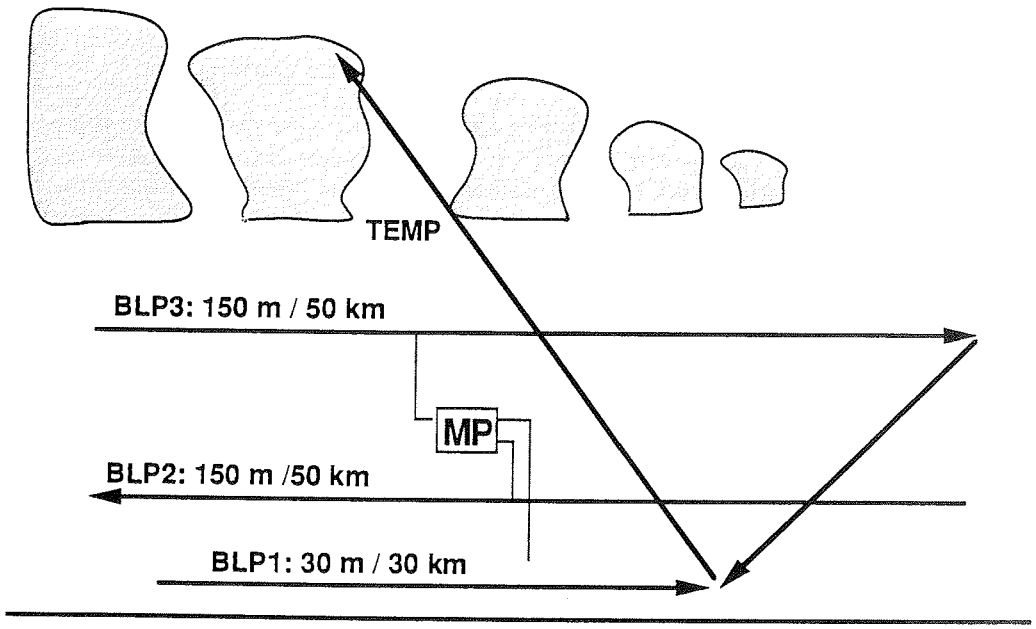

Boundary layer patterns 1,2,3: 15 Oct 91

6 Data Presentation

In this section a few examples of typical features measured during REFLEX I are presented in a preliminary analysis.

6.1 Contrast in Turbulence over Sea Ice and Open Water

The low level flights over sea ice and open water provided data on the different states of turbulent motion in the ABL. As an example, data from two 12 km sections of a level flight in 30 m height (referred to as 'ice section' and 'water section') are shown as time series, and as variance and covariance spectra. Figure 2 shows the time series of vertical wind velocity w', potential temperature θ' and specific humidity q'. The over water and over ice sections are both plotted in the same scale. Mean values of the wind speed, heat flux and moisture flux are listed in Table 1 (refer to Section 5 for details of the synoptic situation).

Table 1: Atmospheric parameters for low level runs on 28 Sep 91. Sensible heat flux H, latent heat flux E, mean potential temperture θ and mean wind velocity U is given.

section	H	E	θ	U
	W/m^2	W/m^2	K	m/s
ice	-2.1	2.2	264.6	9.2
water	70.0	74.3	266.8	12.4

Over open water θ' and q' indicate a convective situation near the surface. Sharp positive deviations from a base level that is somewhat lower than the average calculated over the entire series, lead to a skewed distribution. Both scalar quantities have a remarkably high degree of positive correlation ($r_{\theta q} = 0.88$) indicating a situation of convection in dry, cold air above comparatively warm water. The vertical wind velocity is also positively correlated with θ' and q' ($r_{w\theta} = 0.55, r_{wq} = 0.51$), but does not have such an obviously skewed distribution. In convective situations strong narrow up draughts are surrounded by wider and weaker down draughts, where the skewness is low near the surface and increases with height (Adrian, *et al.*, 1986; Druilhet, *et al.*, 1983).

In contrast, the data from the ice section show rather small deviations from the mean value, especially for θ' and q'. The resolution limit of the sensor is nearly reached and bit-noise becomes apparent.[3] A negative correlation between w' and θ' and also between θ' and q' indicates stable stratification.

Power spectra (Figure 3) and cospectra (Figure 4) of the water section peak at a wavenumber of about $0.003\,m^{-1}$, corresponding to a wavelength of roughly 300 m,

[3]Note that discrete bit steps are somewhat masked due to small fluctuations in pressure, introduced by the calculation of the potential temperature.

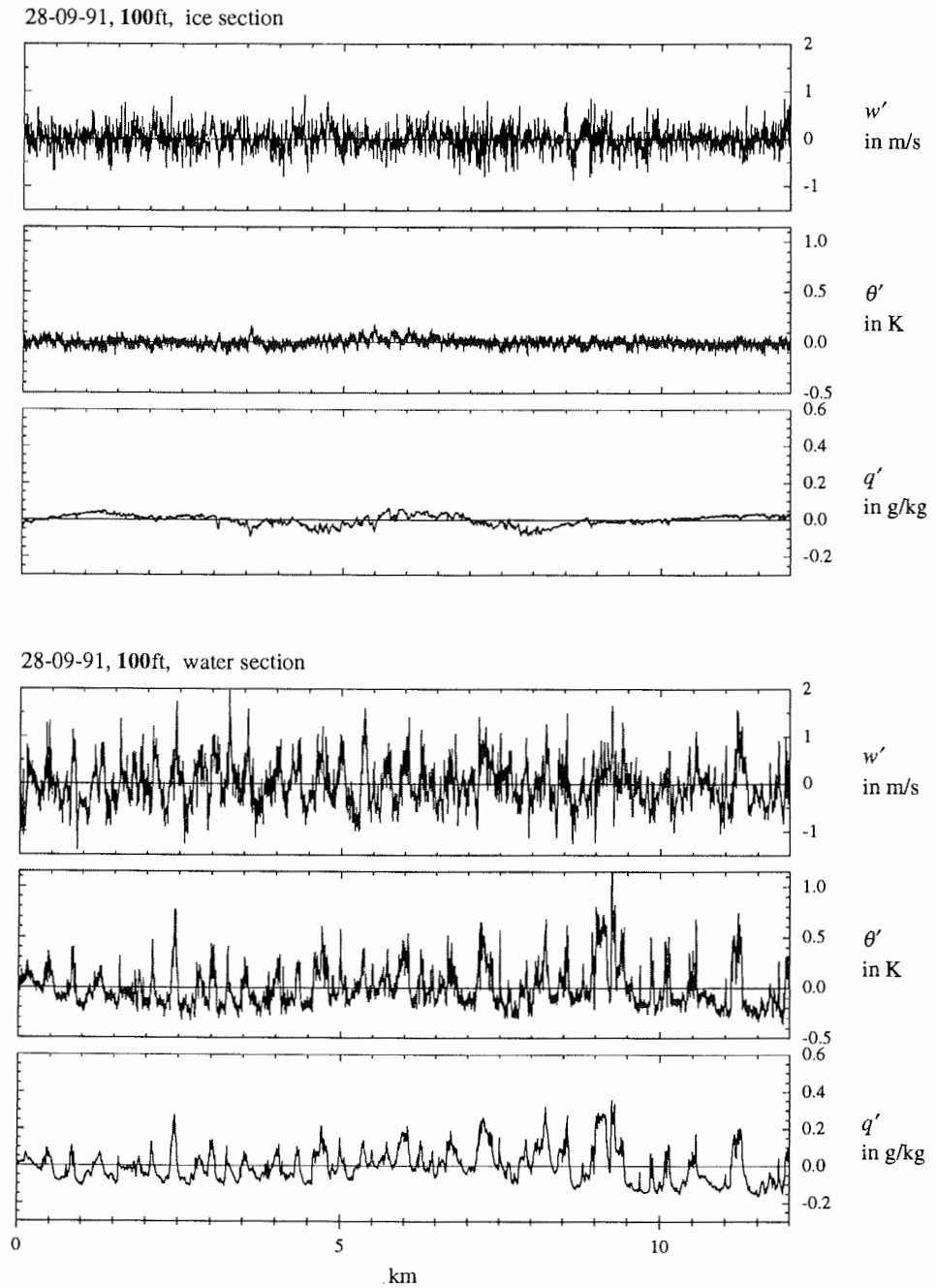

Figure 2: Time series of θ', q' and w' for two 12 km sections of a level flight in 30 m height on 28 Sep 91.

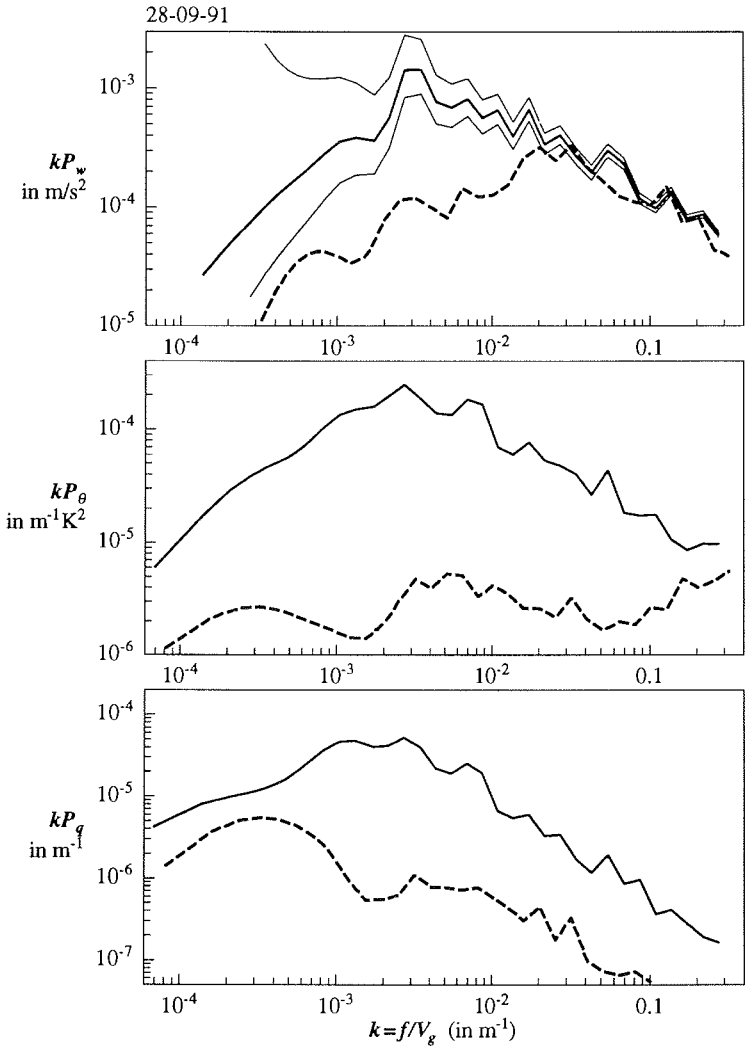

Figure 3: Spectra of vertical wind velocity w', potential temperature θ' and specific humidity q' for two 12 km sections of a level flight in 30 m height on 28 Sep 91. Solid lines are for the open water section, dashed lines for the ice section. f is the frequency, V_g the aircraft speed above ground and P_x the variance spectrum of the quantity x. In the upper graph the 99 % confidence interval, based on the χ^2 distribution is shown by thin solid lines for the open water section.

which is ten times the height above ground. In the ice section w' peaks at roughly 30 m which agrees with purely dynamically generated turbulence. The increase in power for $k \geq 0.1\,\mathrm{m}^{-1}$ of the potential temperature can be explained by bit noise.[4] The cospectra of $w'\theta'$ and $w'q'$ are plotted in energy proportional scaling. Over both sections the latent and the sensible heat flux are of the same magnitude, but

[4]As the curves are multiplied by k, white noise shows as a linear increase with a slope of 1.

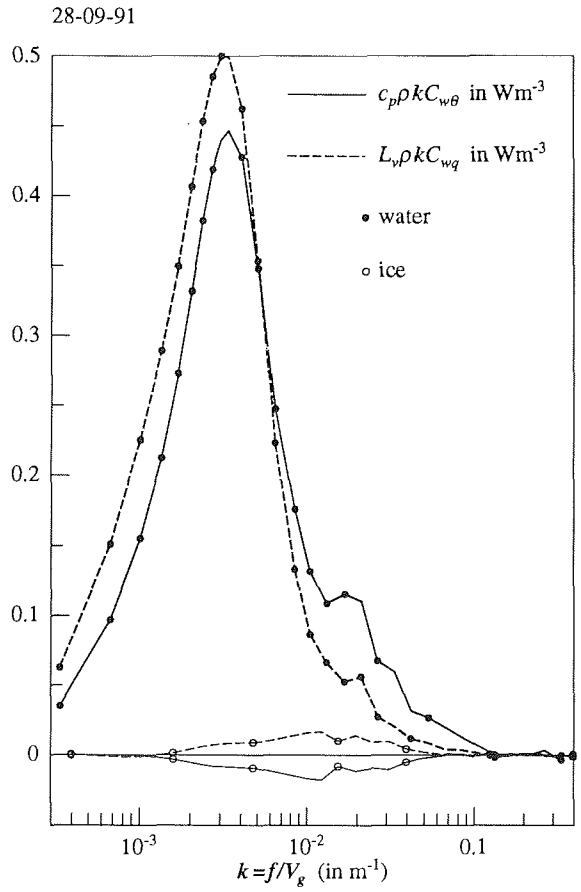

Figure 4: Cospectra of vertical wind velocity w' with potential temperature θ' and with specific humidity q', for two 12 km sections of a level flight in 30 m height on 28 Sep 91. The curves are plotted in energy proportional scaling.

of opposite sign. The latent heat flux spectrum virtually mirrors that of the sensible heat flux, reflecting opposite mean vertical gradients of humidity and potential temperature.

6.2 Roll Vortex Motion

In cold, arctic air masses flowing over open water, convection frequently organises into roll vortex motion with the roll axes roughly parallel to the mean wind direction. During REFLEX I this regime was encountered on three days and could be recorded in detail by several flights across the roll axes, ascents and descents between the surface and the top of the inversion, and by a series of drop sondes. Data from

the observation on 14 October 91 are shown as spectra (Figure 5) and space series (Figure 6). Three runs were flown at distances of 17, 41 and 93 km from the ice edge in heights of 54 m, 87 m and 155 m, respectively. Refer to Section 5 for a sketch of the flight pattern and details on the synoptic situation.

Evidence of roll vortex motion in the spectra of turbulence quantities is given by

- a peak in the horizontal wind component orthogonal to the mean wind direction,
- a significant contribution to the fluxes of heat and moisture in a wavelength band considerably larger than that of convective turbulence (which is near the surface at 3 to 6 times the height above ground or in the middle of the mixed layer 3 to 6 times the mixed layer height, z_i).
- a 90° phase shift between the vertical wind component and the one orthogonal to the mean wind, along with a significant coherence between these two components.

In Figure 5 spectra for each of the three runs are shown. A shaded area indicates the wavelength band for which the above conditions for roll vortices are best fulfilled. This band is in the range of $0.7\,\mathrm{km} < \lambda < 1.7\,\mathrm{km}$ for the run nearest to the ice edge, and moves to larger wave lengths with increasing distance from the ice edge, reaching $2.0\,\mathrm{km} < \lambda < 7.0\,\mathrm{km}$ for the third run. Runs that have been flown in the eastward direction are reversed so that the phase shift can be interpreted in a geographical sense. A phase shift ϕ_{wu} of -90° means w leads u. Thus, a point with a maximum in w has a minimum in the u-component (i.e. $u < 0$) to the east, and a maximum in the u-component (i.e. $u > 0$) to the west.

Table 2: Atmospheric parameters for the cross wind runs on 14 Oct 91. The table lists sensible heat flux H, latent heat flux E, mean potential temperture θ, height h, and distance from the ice edge Δx.

run	H	E	θ	h	Δx
	$\mathrm{W/m^2}$	$\mathrm{W/m^2}$	K	m	km
1	180.5	137.5	257.4	54	17
2	159.2	138.8	259.3	87	41
3	96.6	100.6	261.7	155	93

An excerpt of the run nearest to the ice edge is shown in Figure 6. All three components were band-pass filtered to leave only the wavelength band of high coherence between the w and u wind components, as marked in Figure 5. In these two components the roll vortex motion is evident as a regular pattern. Temperature and humidity maxima correlate with upward motion.

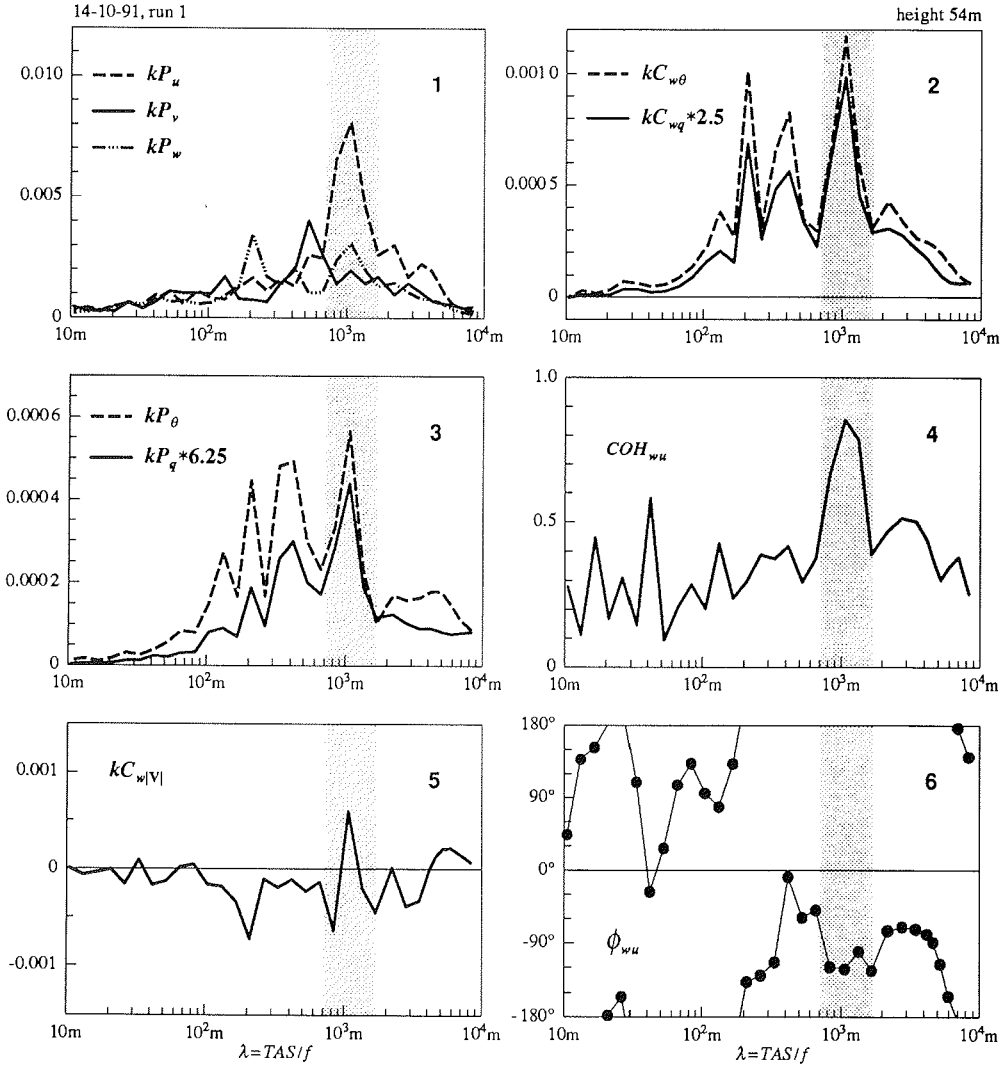

Figure 5: Spectra of turbulence quantities for three runs over open water (Figures a–c) across roll circulation on 14 Oct 91. The abscissa is the wavelength λ in metres, TAS the airspeed and f the frequency. The six graphs show:

1 variance spectra of the three wind components in the meteorological system (u positive towards east, v positive towards north and w positive upwards). Since the mean wind direction is north, the u-component is orthogonal to the roll axes. The dimensions are m^2s^{-2}.

(continued)

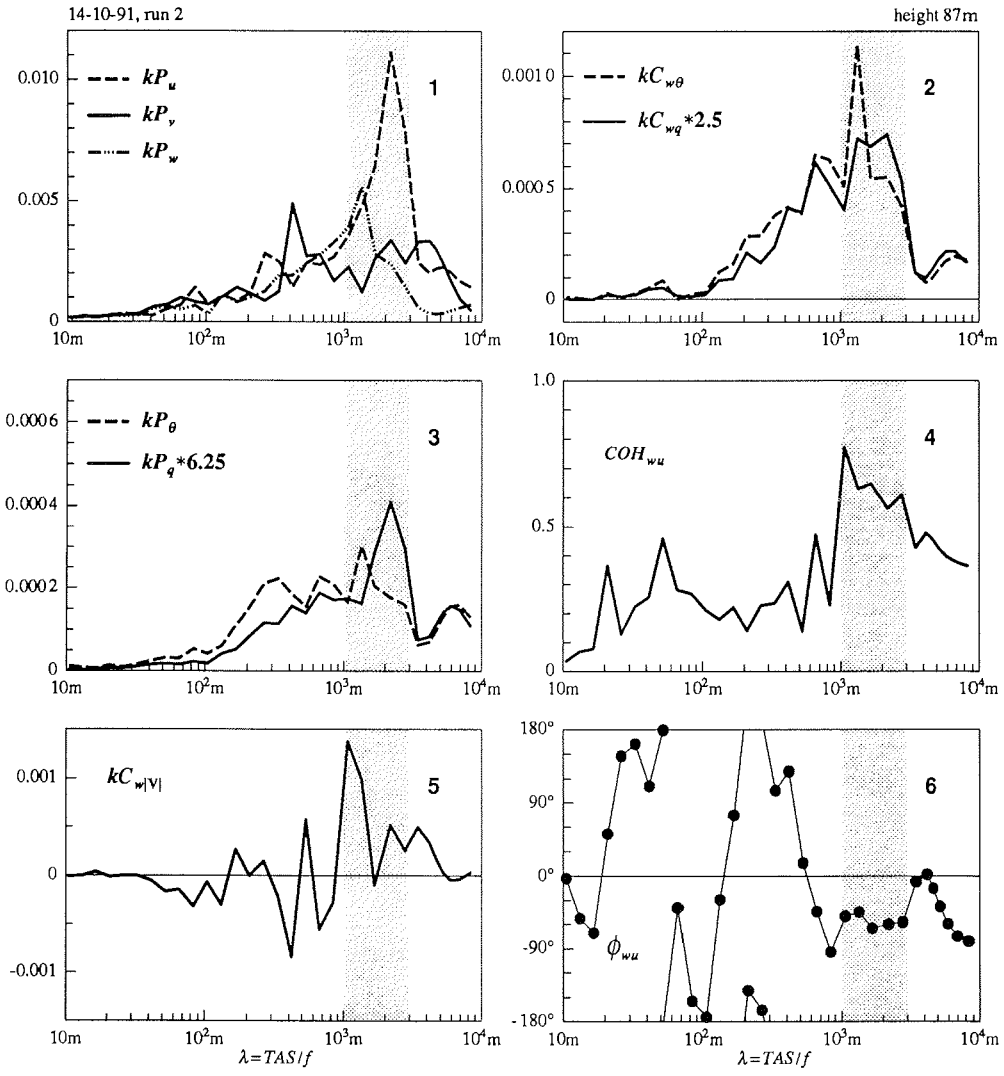

Figure 5b: (continued)

2 cospectra of sensible and latent heat flux plotted such that the area under the curve is proportional to the energy flux. The dimensions are $m^2s^{-1}K$ for $kC_{w\theta}$ and $m^2s^{-1}gkg^{-1}$ for kC_{wq}.

(continued)

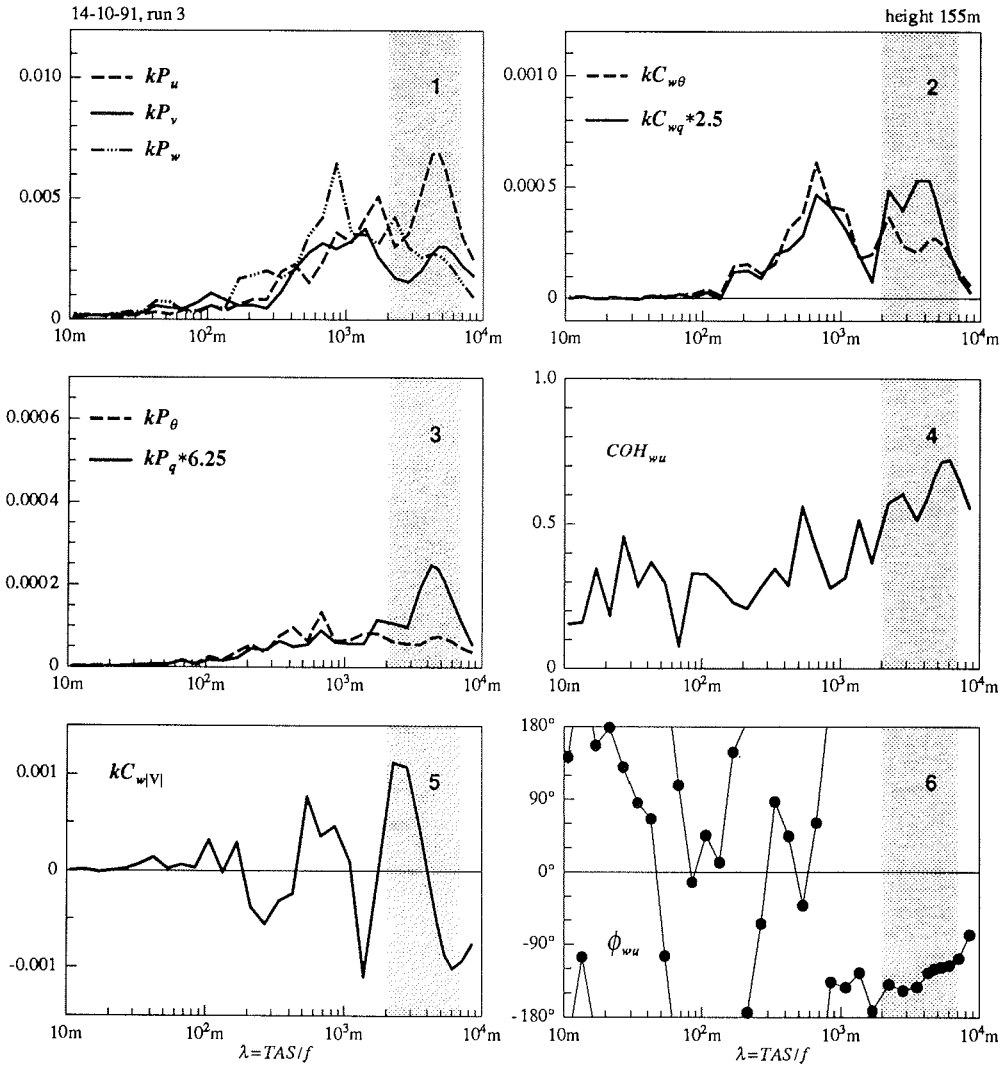

Figure 5c: (continued)

3 variance spectra of the potential temperature and specific humidity, plotted in variance proportional scale. The humidity spectrum is multiplied by 6.25 in order to appear in the same relative magnitude as the temperature spectrum with respect to their contributions to the turbulent energy flux. The dimensions are mK^2 for kP_θ and mg^2kg^{-2} for kP_q.

4 spectrum of the coherence between the w and u wind components.

5 cospectrum of the shear stress, defined as $w'(\sqrt{u^2+v^2})'$.

6 phase spectrum of w and u.

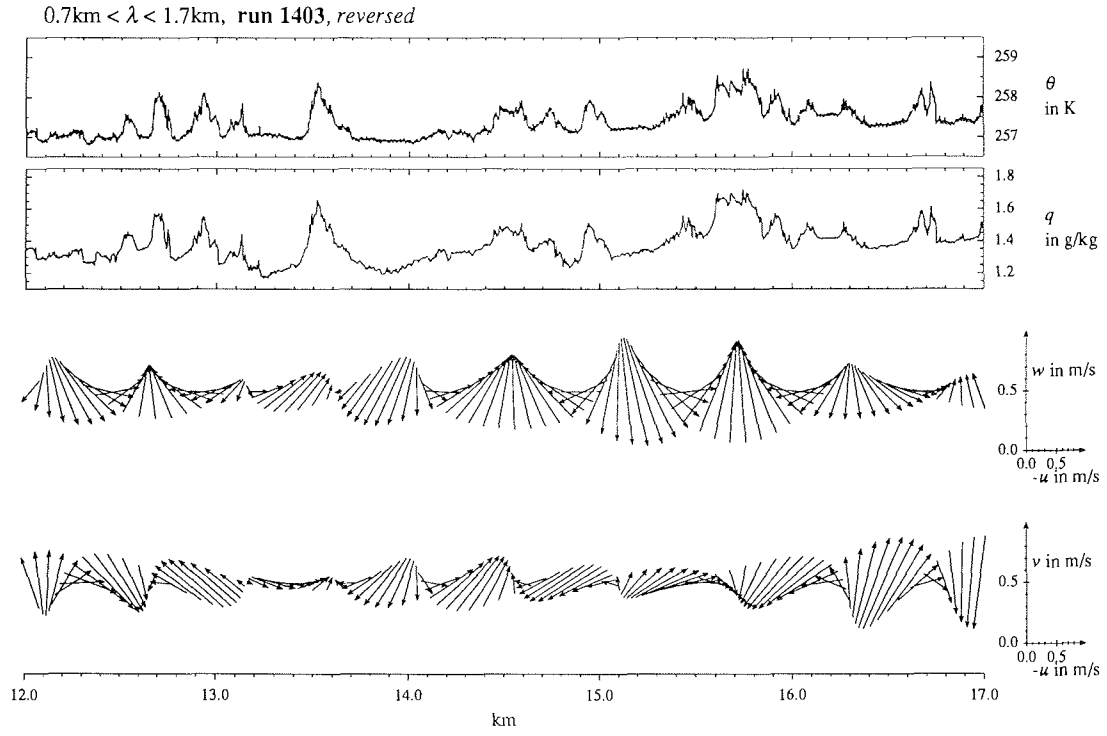

Figure 6: Time series of potential temperature θ, specific humidity q and the wind components, plotted as arrows in the $x - z$ and $x - y$ planes. The data are an excerpt of run 1 on 14 Oct 91.
The abscissa gives the distance from the eastern end of the run. The wind components have been band-pass filtered to leave only the wavelength band with high coherence between w and u, as marked in Figure 5. Temperature and humidity are not filtered.

6.3 Analysis of Surface Structure from LSC Data

6.3.1 Data analysis

After correction for vignetting an interactive dynamic threshold method is applied to frames consisting of 704 single lines to identify the three surface conditions ice, nilas and water. The method reduces the number of different grey levels from 255 to three. Percentages of coverage for each of these surface conditions are then calculated for single lines and for fields of 500 or 1000 lines.

Characteristic floe sizes are found by calculating a size distribution $g(p)$ of ice sections in each single line orthogonal to the flight path. Here, p is the floe size in number of pixels, and $g(p)$ (dimension 1/pixel) the number of floes of size p. These distributions are summed over 1024 successive lines, corresponding to an area of 3 km by 3 km. Note that the algorithm does not actually identify the area of individual floes, but rather finds the length of chords with which the scan lines cut the floe. If we assume the floes are of the same length in the direction orthogonal and parallel to the flight path, the number density distribution $f(d)$ (the number of floes of size d (in m) per unit area, $d = pl_\perp$) is given by

$$f(d) = \frac{1}{p}\,\frac{l_\parallel}{l_\perp}\,g(p)\,\frac{1}{A},$$

where $l_\parallel$ and $l_\perp$ are the lengths that one pixel represents in the direction parallel and orthogonal, respectively, to the flight path, and A is the area in m^2 scanned by 1024 lines.

The characteristic floe size is then defined as the mode d_m of $d^2 f(d)$, the area density distribution, thus corresponding to floes with the highest relative area coverage. For perfectly circular floes d_m underestimates the floe diameter by a factor $\frac{\pi}{4}$.

In order to investigate the geometry of floes the algorithm described above is also applied after rotating the 1024×1024 pixels field by 90°. The such obtained spectra are referred to as parallel.

6.3.2 Examples of LSC data

The following series of Figures 7 a-h were recorded on 22 September 1991 north of Svalbard during an 80 km long flight section at a height of 3100 m from the ice edge into the pack-ice. Each picture has a width of 3 km and a length of 2 km, covering an area of 6 km^2. The series shows different floe sizes and ice concentrations on the track from south to north during on-ice winds and cloudless sky. The most relevant structures of the ice fields are discussed in the figure captions.

The distribution of water, nilas and snow covered ice is shown in Figure 8. Compact ice fields are observed close to the ice edge (km 7 – 15). Between 20 and 35 km from

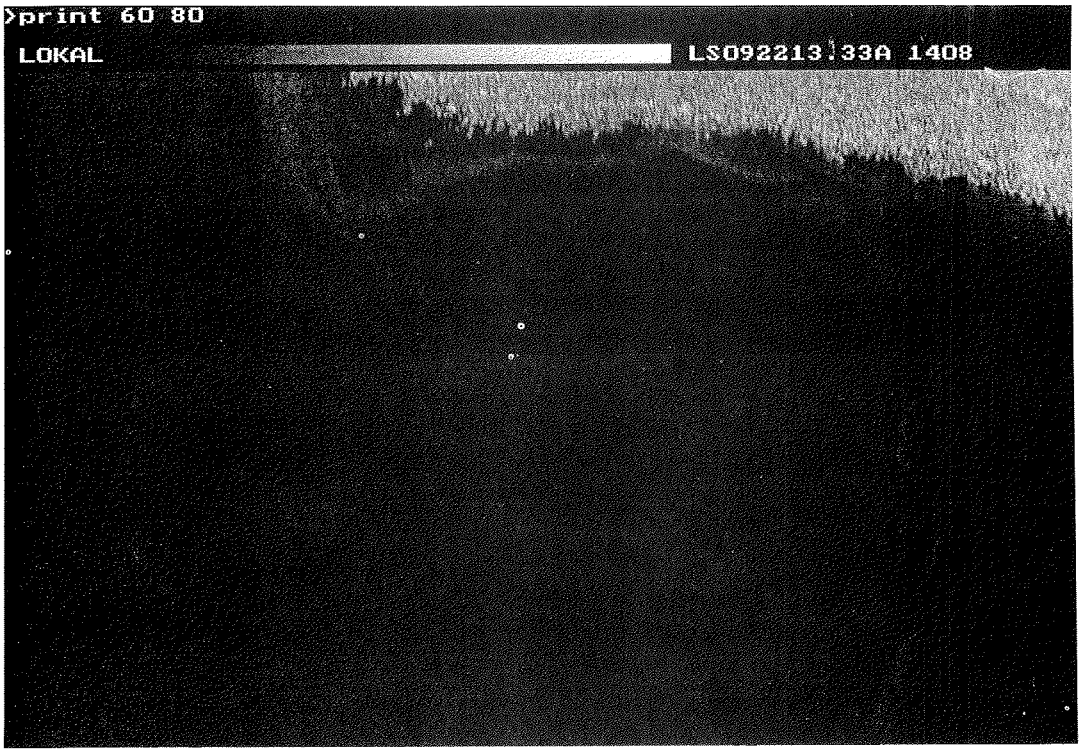

Figure 7: A series of LSC pictures (a-h) showing different sizes, concentrations and structures of ice floes. The pictures are recorded on 22 Sep 91 during a northbound flight at 3000 m height. Percentages of open water, nilas and ice, denoted by W, N and I, respectively, are given for each picture.
a: Compressed ice edge in the upper part of the figure with a band of grease ice on the water surface. W: 93.0%, N: 2.5%, I: 4.5%.

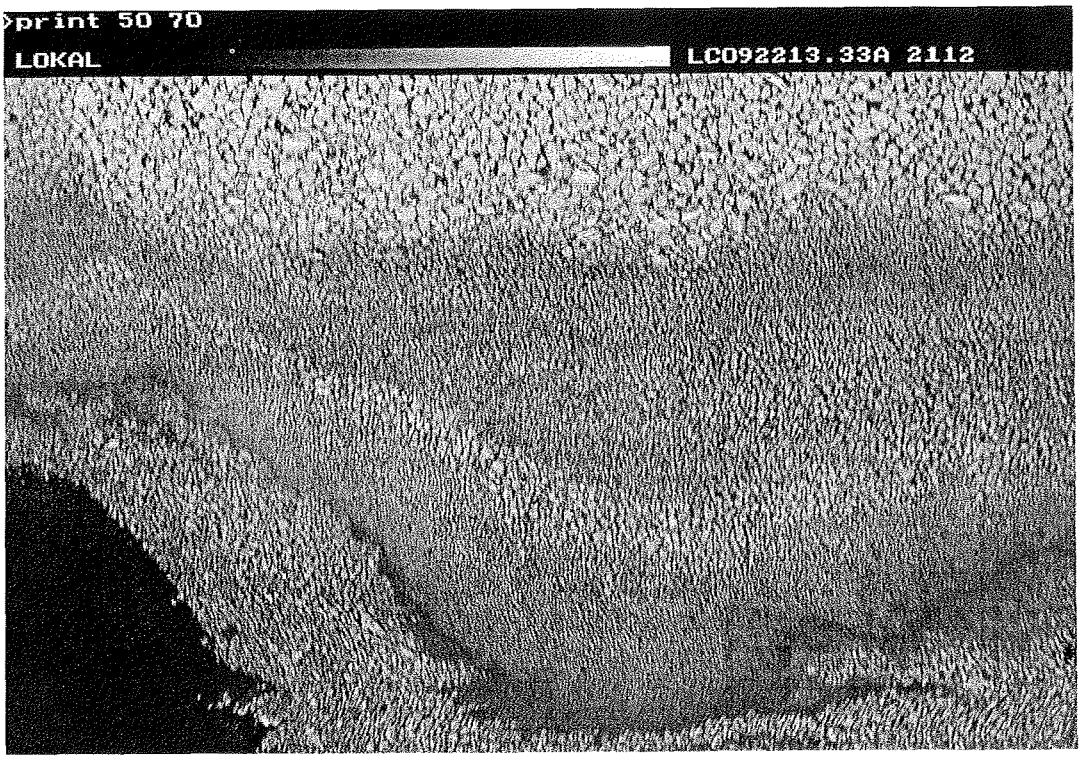

Figure 7 b: Pancake ice and ice fragments in the lower part of the picture, snow covered small ice floes in the upper part. W: 7.8%, N: 10.6%, I: 81.6%.

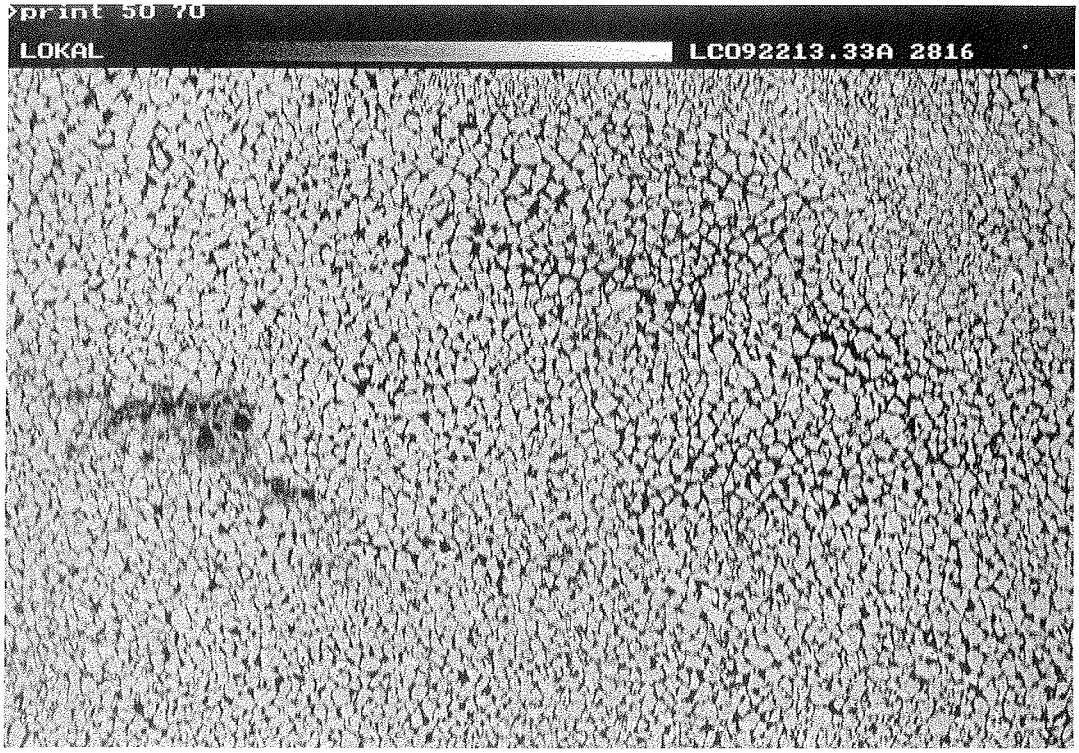

Figure 7 c: Compressed ice floes with a typical diameter of 20 m, with a patch of flooded and refrozen floes (left). W: 0.3%, N: 7.3%, I: 92.4%.

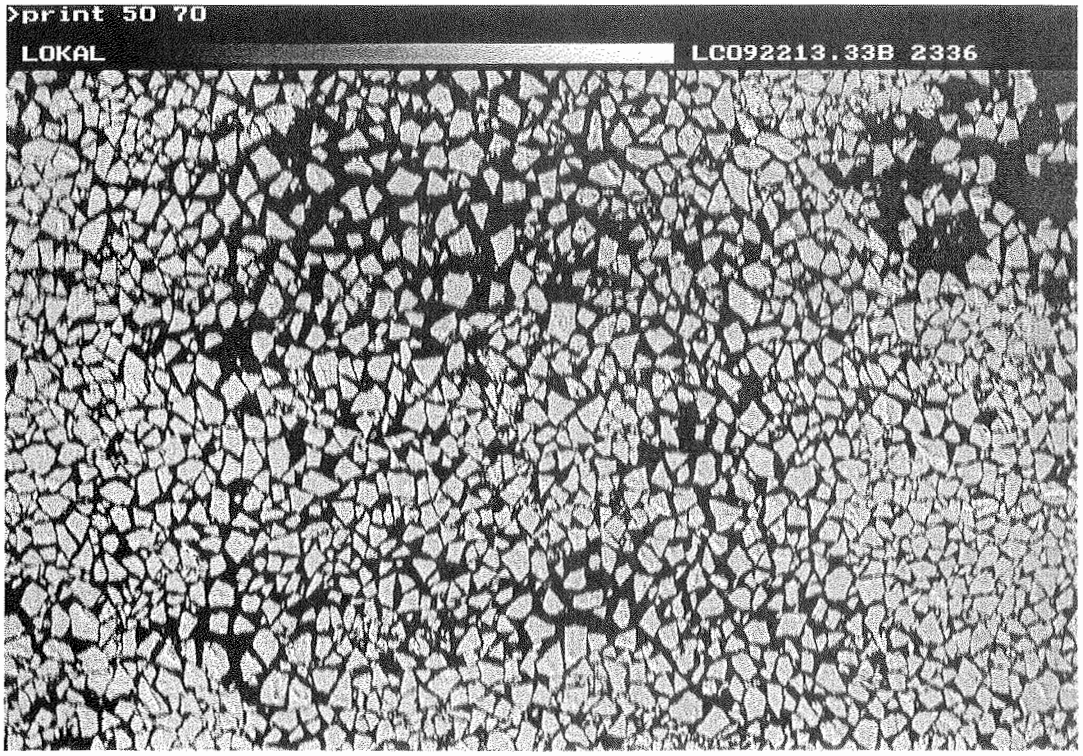

Figure 7 d1: Loose snow covered ice floes, about 18 km from the ice edge. W: 22.9%, N: 19.5%, I: 57.6%.

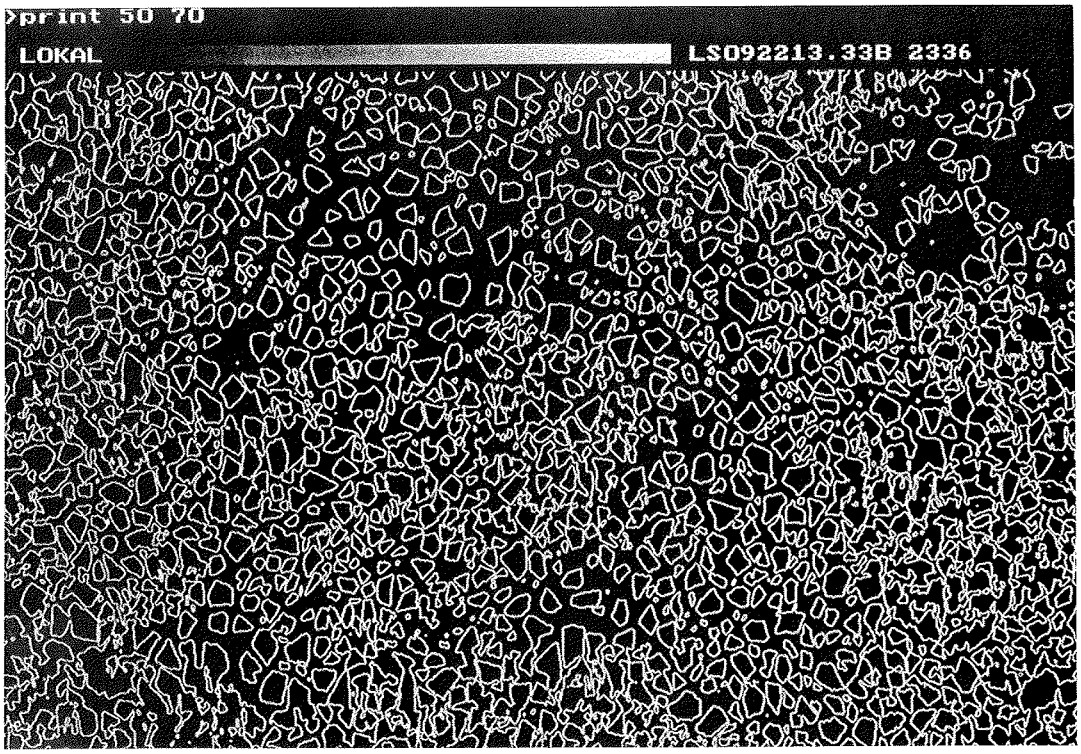

Figure 7 d2: Display of ice floe borders. The picture is created by further segmenting the three different grey levels into two, representing 1) water and nilas and 2) ice. Each pixel that has a direct neighbour of different value is then marked white, while all others are marked black.

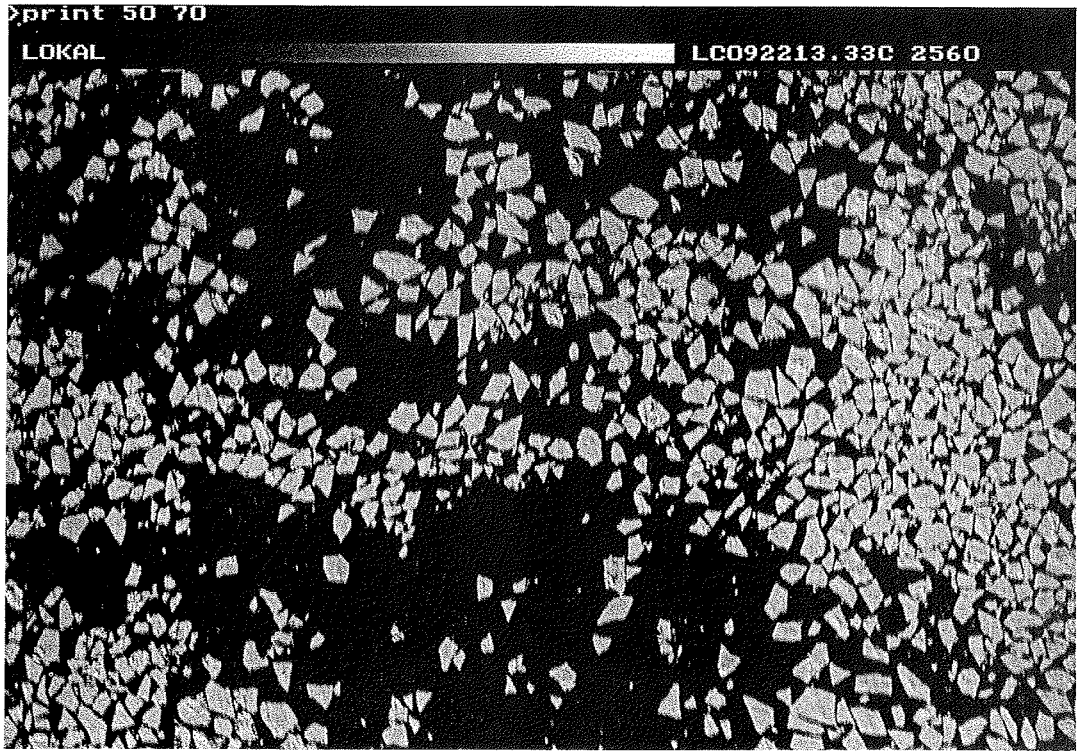

Figure 7 e: Very loose ice fields with maximum floe size of 120 by 70 m, located 30 km north of the ice edge. W: 53.4%, N: 10.7%, I: 35.9%.

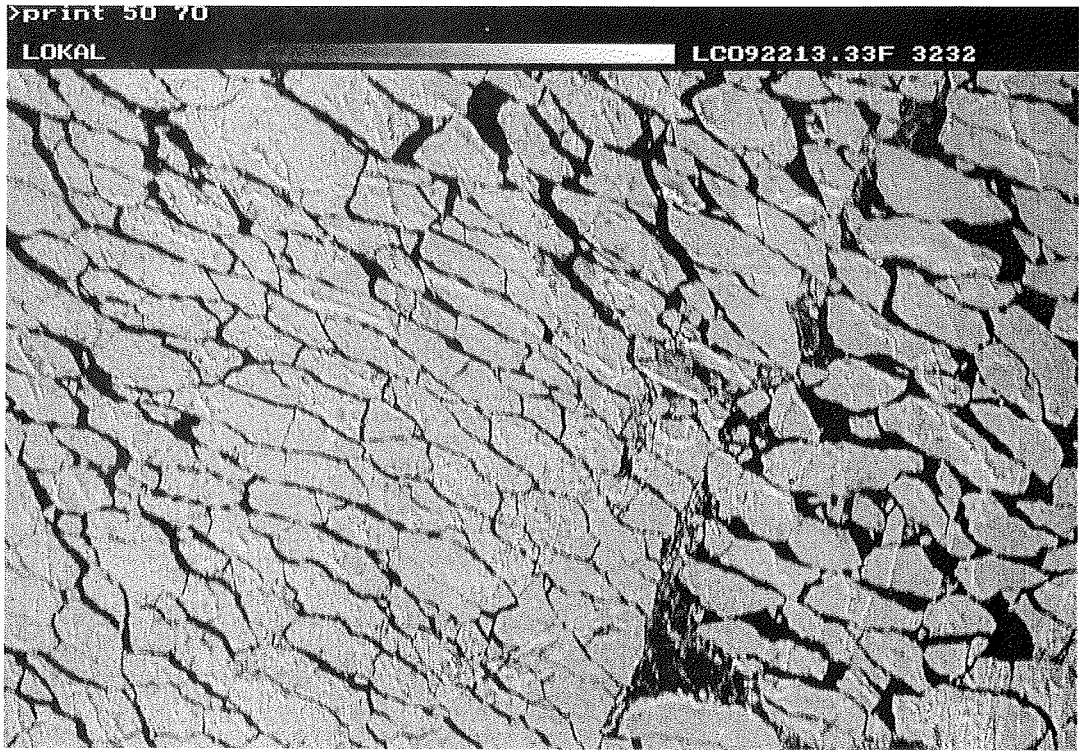

Figure 7 f: Compact, swell-broken, old ice floes, 70 km from the ice edge. W: 5.2%, N: 9.7%, I: 85.1%.

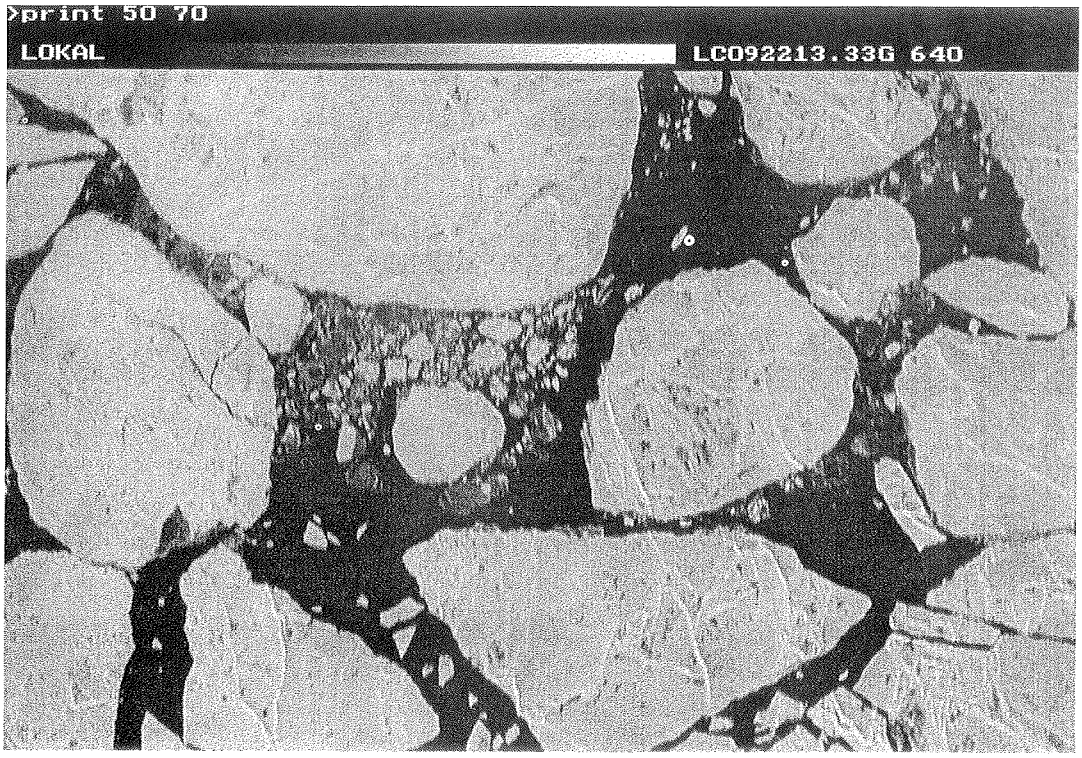

Figure 7 g: Large and smaller broken old ice floes covered with ice ridges, 75 km from the ice edge. W: 16.3%, N: 8.7%, I: 75.0%.

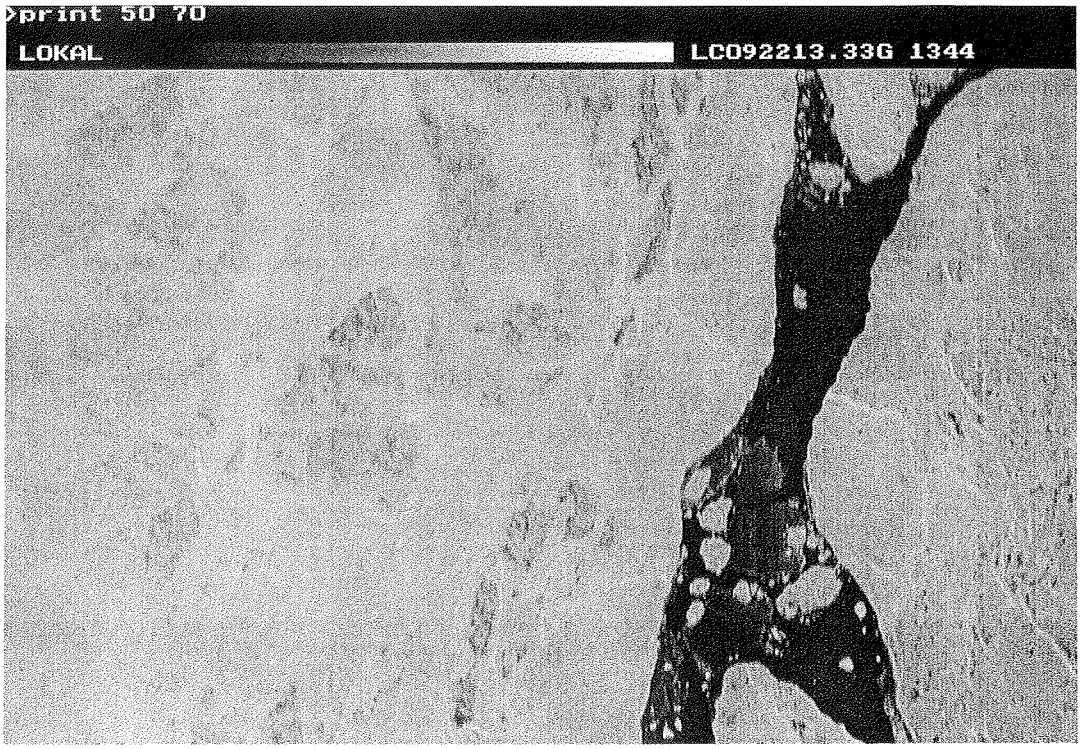

Figure 7 h: Large ice floe (left), covered with melt puddles and new ice (nilas) formation in the lead between two huge floes; nearly 80 km from the ice edge. W: 5.8%, N: 3.5%, I: 90.7%.

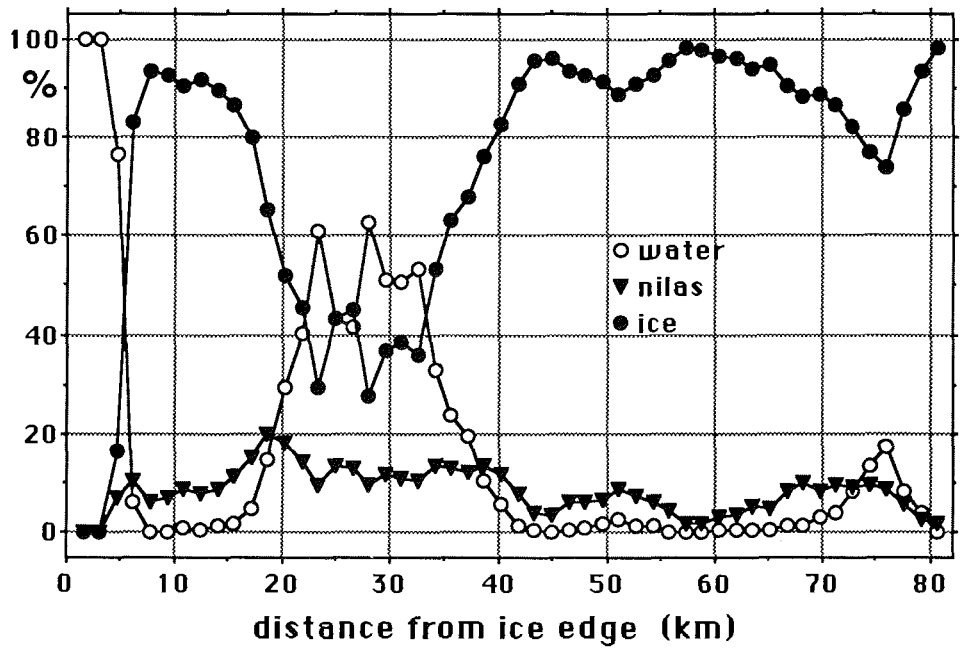

Figure 8: Percentage of open water, nilas and ice as a function of distance from ice edge, northbound flight in 3100 m on 22 Sep 91.

the ice edge, ice concentration is reduced to 45%, most likely as a result of divergence in the wind field. Higher ice concentrations reaching nearly 100% are found in the interior pack ice. Typical nilas concentrations are below 20% with a mean value of 8.4%.

Floe size distributions $d^2 f(d)$ corresponding to Figures 7 c, d, e, f, are presented in Figure 9. A distinct peak in the spectra shifts from values of 25 m close to the ice edge to 120 m in the interior pack ice region south of the large old ice flows.

The characteristic scales of floes show a gradual increase from about 50 m close to the ice edge to more than 100 m in the pack ice (Figure 10), and a rather steep increase at 70 km. Within the limits of accuracy no significant difference can be found in the characteristic size derived from the distribution calculated orthogonal and parallel to the flight path.

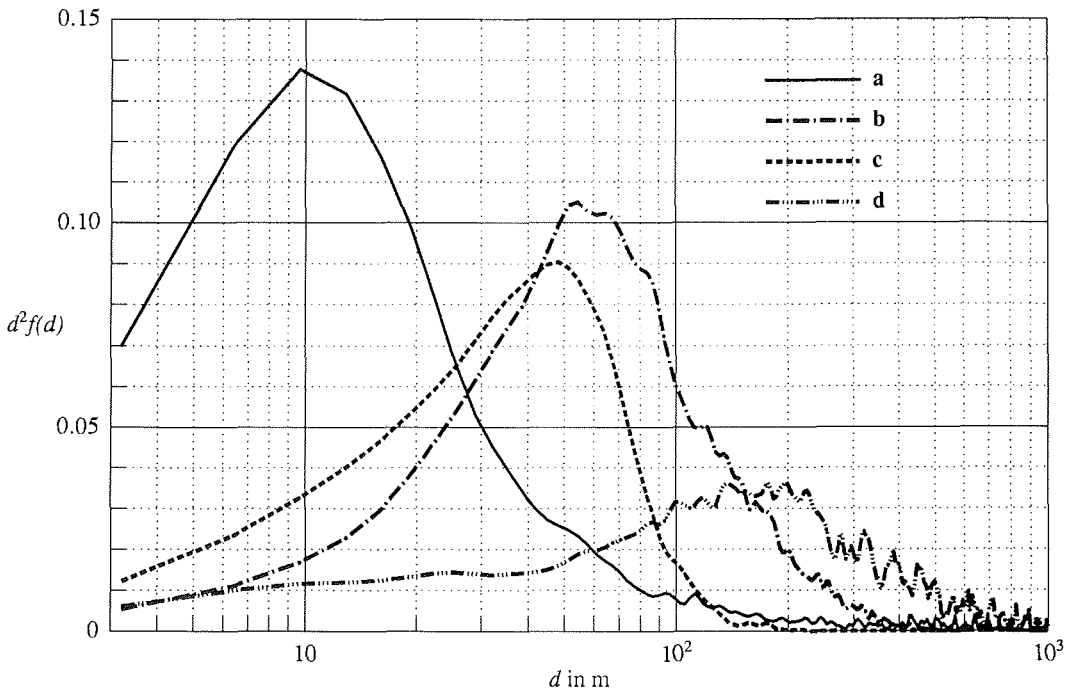

Figure 9: Distribution of floe sizes, corresponding to Figures 7 c, d, e, f.

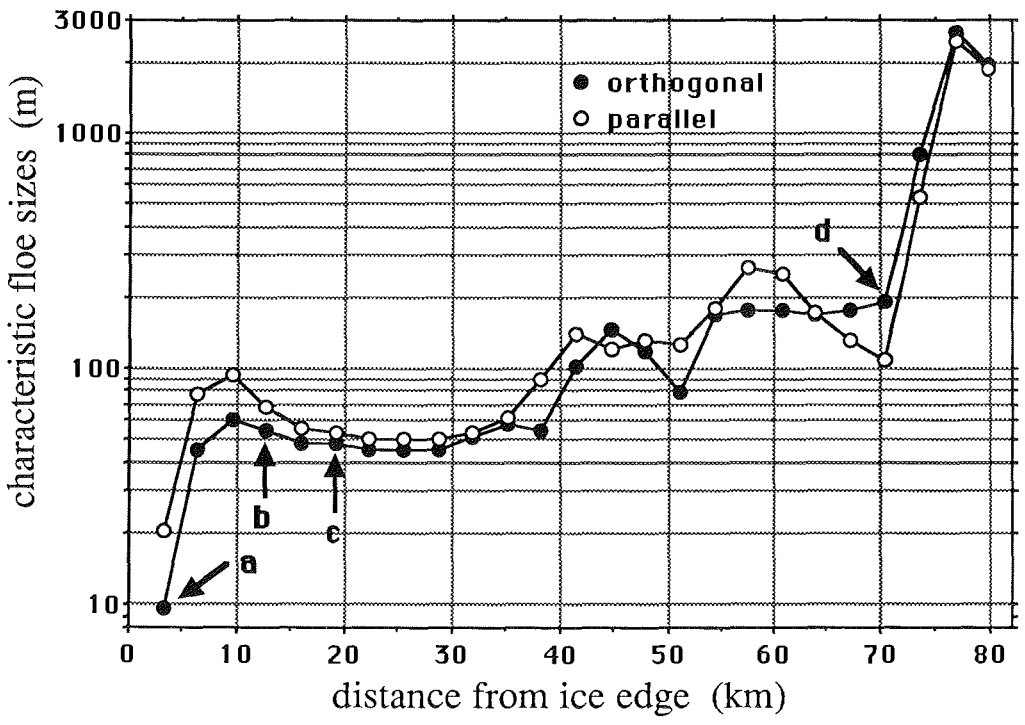

Figure 10: Characteristic floe sizes parallel and orthogonal to the flight direction as a function of distance from the ice edge.

6.4 Relation between Surface Structure and Airborne Measurements

Measurements during low level flights parallel to the mean wind direction are used to study correlations between turbulence parameters and water/nilas/ice distributions. Percentages of coverage of open water and ice were calculated for each scan line separately, corresponding to a band of 30 m width orthogonal and 2 m width parallel to the aircraft track. Figure 11 shows an excerpt of a run from a north bound flight section with northerly winds, carried out on 26 September 1991. The ice concentration data were synchronised with the turbulence and radiation data by aligning corresponding changes in the KT4- and the LSC-signals generated by floe edges. The flux data shown in Figure 11 were calculated by applying a high-pass filter to u, v, w, θ and q to form the prime quantities, and a low-pass filter to the instantaneous fluxes. Both filters had a cut-off frequency that corresponds to a wave length of 1 km.

Even if the correlations are affected by differences in response behaviour and viewing angle, a high level of agreement exists between the different radiation signals. The flux data also reflect the surface characteristics. However, a few features attract attention:

- The maximum values of the surface temperature (KT4) are approximately 0.7 K lower than the freezing temperature of sea water. This can be explained by an emissivity of the water of less than 1, the value assumed in the calibration of the instrument. Furthermore grease ice bands were observed in leads opened by the cold off-ice airflow. The surface temperature of the grease ice can be lower than -1.8°C, lowering the area average of the KT4 measurement.
- The albedo of the ice surface increases from a value of 80% at the beginning to over 90% towards the end of the run and mirrors to a certain degree the minimum values of the KT4. Possible explanations include the limited accuracy with which small radiative fluxes can be measured (leading to relatively large errors in the quotient of two small numbers) and atmospheric effects due to a small incident angle of the solar radiation. An inhomogeneous cloud cover may then lead to locally higher radiation at the surface than at flying altitude. At this stage of the data analysis an explanation cannot yet be given.
- Latent and sensible heat fluxes are very similar, as observed in the over water part reported in Section 6.1 (cf. Figure 4). The magnitude of the momentum flux is also very similar to the turbulent energy fluxes, suggesting that the thermodynamic effect dominates the turbulence structure.

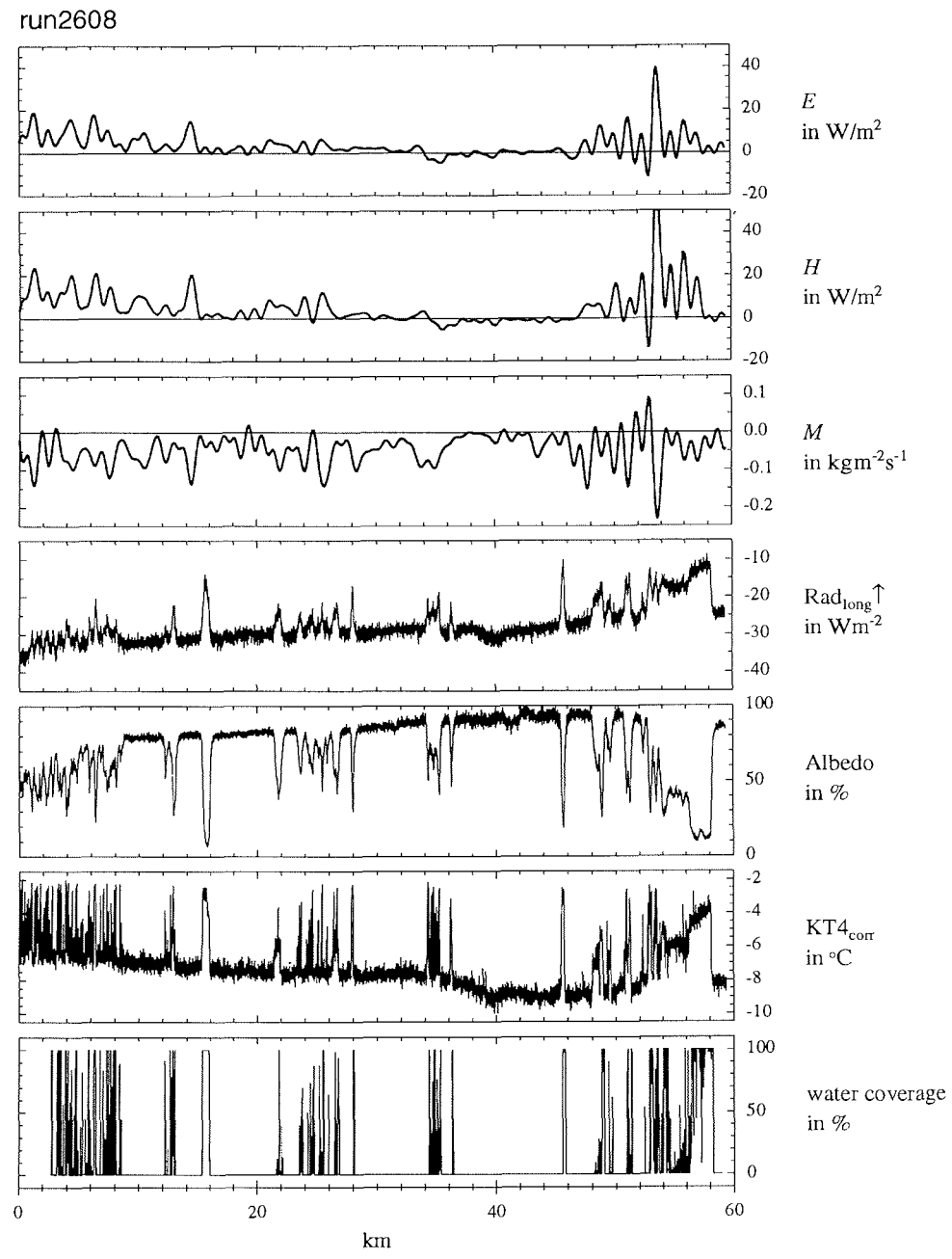

Figure 11: Time series of radiation and turbulence data and percentage of open water determined from the Line Scan Camera. The data are from a 30 m northbound run under off-ice conditions on 26 Sep 91. E is the latent heat flux, H the sensible heat flux, M the momentum flux, $\mathrm{Rad}_{\mathrm{long}}\uparrow$ the upwelling long-wave radiative flux and $\mathrm{KT4}_{\mathrm{corr}}$ the corrected surface temperature.

7 Acknowledgements

Thanks are due to the pilots, engineers and technical staff who supported this experiment and contributed with their effort and commitment to making REFLEX I a success.

8 References

Adrian, R.J., Ferreira, R.T.D.S and T. Boberg, 1986: Turbulent thermal convection in wide horizontal fluid layers. *Experiments in Fluids* **4**, 121–141.

Bochert, A., 1991: *Linecalc 1.0 Systemhandbuch*, Alfred-Wegener-Institut für Polar- und Meeresforschung, August 1991.

Druilhet, J.P., Frangi, P., Guedalia, D. and J. Fontan, 1983: Experimental Studies of the Turbulence Structure Parameters of the Convective Boundary Layer. *J. Climate Appl. Meteor.* **22**, 594–608.

Vörsman, P., Friederici, B. and A. M. Hoff, 1989: METEOPOD – ein flugzeuggestütztes Turbulenzmeßsystem, *Promet* **1/2** 1989, 57–64.

Wamser, C. and El Naggar, S., 1989: Line Scan Camera Measurements. *Hamburger Geophysikalische Einzelschriften*, ARKTIS 1988, Field Phase Report, 57–60.